

Optical Fibre Communications Between Radio Telescopes in the European VLBI Network

TMR-LSF RTD Sub Project 4

**Dr. Brian Smith
Dr. R. E. Spencer
Mr. D. C. Brown
Dr. M. Bentley
Jodrell Bank Observatory
University of Manchester
Cheshire, UK**

June 2000

EXECUTIVE SUMMARY

The increase in availability of installed optical fibre within Europe is presenting a unique opportunity to upgrade the European Very Long Baseline Interferometry Network (EVN). This network of European radio observatories regularly take part in joint sessions to observe celestial radio sources at high resolution, using sophisticated magnetic tape equipment to record data at rates up to 1 Gbit/sec. There are clear advantages to replacing the current recorder technology with an optical fibre network. These include earlier availability of scientific results and perhaps more importantly, increased efficiency during the observing sessions.

This report investigates the feasibility of interconnecting the EVN with optical fibres. The work involves the construction of optical device and system models in MATLAB script for both analogue and digitally modulated optical links. These models are used to predict the performance of optical links over distances in excess of 3000km, taking account of chromatic dispersion, non-linear phenomena such as SBS and polarisation mode dispersion if appropriate. In addition to the theoretical modelling, experimental work is performed to verify the models and better characterise phase instabilities for the analogue case. Furthermore, contact has been made with the optical fibre industry to investigate the availability of dark fibre across the EVN span and close to the VLBI station sites leading to cost estimates for both a single experimental link and full network implementation.

The work predicts that digital modulation should be the preferred option over analogue for optical fibre links over distances up to 3000km. Commercial equipment is already available which can provide multi-wavelength long haul optical fibre links at speeds up to 10Gbps per wavelength and fibre is, and will become available within continental Europe to provide a backbone for this communication link.

In conclusion we find that the connection of VLBI observatories in EVN to a central correlator at 1 Gbit/sec or higher data rates is certainly feasible with fibre optic technology. Current costs using installed fibre are probably prohibitive. However plans for a very high data rate system to connect European large scale facilities and academic institutions make could make such a system affordable in future.

The report consists of the main part (sections 1 to 11) and three appendices.

1. INTRODUCTION.....	5
1.1 Background and Scope.....	5
1.2 General System Outline.....	6
1.3 Structure of the Report.....	7
2. SPECIFICATION AND DEFINITION OF PARAMETERS.....	8
2.1 System specifications.....	8
3. CURRENT STATUS OF OPTICAL COMPONENTS.....	9
3.1 Lasers.....	9
3.2 Modulators.....	11
3.3 Integrated Transmitters.....	13
3.4 Photodiodes.....	13
3.5 Optical Interfaces.....	15
3.6 Optical amplifiers.....	15
4. OPTICAL LINK MODEL DEVELOPMENT.....	18
4.1 Analogue Optical Links.....	18
4.1.1 System Definitions.....	18
4.1.2 Evolution of Signal and Noise in Analogue Optical Systems.....	19
4.1.3 Optical Amplifier Noise.....	21
4.1.4 Optical Amplifier Saturation.....	22
4.1.5 Determination of Performance Metrics for Analogue Systems.....	23
4.1.6 Chromatic Dispersion in Analogue Optical Links.....	26
4.1.7 Effects of Stimulated Brillouin Scattering on Analogue Optical Systems..	28
4.2 Digital Optical Links.....	29
4.2.1 Signal Formats.....	29
4.2.2 Noise in Detection Processes.....	30
4.2.3 Bit Error Rate (BER).....	31
4.2.4 Performance of Optical Amplifiers in Digital Optical Links.....	33
4.2.5 Example Optical Link without Optical Amplification.....	33
4.2.6 Modelling Chromatic Dispersion in Digital Optical Links.....	34
4.2.7 Polarisation Mode Dispersion in Digital Optical Links.....	35
4.3 Development of MATLAB Graphical User Interfaces (GUIs).....	37
5. ANALYSIS AND PERFORMANCE OF ANALOGUE OPTICAL LINKS.....	38
6. ANALYSIS AND PERFORMANCE OF DIGITAL OPTICAL LINKS.....	40
7. EXPERIMENTAL MEASUREMENTS AND VERIFICATION.....	42
7.1 Introduction.....	42
7.2 Measurement of V_{π} of Optical Modulator.....	42
7.3 Comparison Between System Experiments and Simulation.....	43
7.4 Experimental Verification of Dispersion Characteristics.....	46
7.5 Experimental Phase Stability Measurements.....	47

8. EXAMPLE LINK : PERFORMANCE AND COST ISSUES	50
9. IMPLEMENTATION ISSUES	52
9.1 Pre-Installed Leased Dark Fibre	52
9.2 Self-Build Option	52
9.3 Available Optical Fibre Capacity Within Europe	53
9.4 Full Network Costs.....	55
10. CONCLUSIONS	59
11. REFERENCES	61

APPENDICES:

- A. Phase Performance of Fibre Links
- B. The SDH and SONET Standards
- C. Transfer of VLBI Signals to SDH

1. INTRODUCTION

1.1 Background and Scope

Very Long Baseline Interferometry (VLBI) is an aperture synthesis technique which allows radio astronomy measurements to be performed on a continental or global scale. Baselines between 100 and 9000km can be achieved providing the highest angular resolution of any branch of astronomy and enabling imaging at angular scales as small as 100 microarcseconds. Within the European VLBI Network (EVN) there are fourteen telescopes located from Finland to central Spain, to the southernmost tip of Italy and to the Ukraine and China with a maximum baseline capability of approximately 9000km. This report will not consider the Ukrainian or Chinese telescopes.

VLBI is achieved over such large spans using tape recording technology. Data is recorded onto large reels of video tape during an observing session. Tapes are then played back at a central correlator (in Europe these are situated at JIVE, Dwingeloo Holland or at MPI Bonn, Germany) where the data is effectively multiplied together to produce interference fringes for each interferometer pair. Due to the necessary delays in shipment and correlation, VLBI observers do not know whether their experiments have been successful until some time after the event.

Magnetic recording at remote sites is currently limited to a maximum data rate of around 1Gbps using the latest MkIV technology. The recording and playback apparatus is unique to radio astronomy and is designed and built specifically for this application. For this reason, development costs are high and maintenance is manpower intensive at each of the sites. In addition to this, the scheduling and re-scheduling of measurements is logistically complex and problems with recording apparatus can lead to more than 10% data loss during any measurement. In terms of scientific measurements, researchers can wait up to six months for results under the present system and so a real time alternative would lead to more rapid dissemination of results from the European VLBI consortium.

The explosion of the global internet market and the associated increase in installed optical fibre capacity presents an opportunity to replace existing inefficient recording technologies with real time interconnection between each of the sites and the correlator. Indeed several radio astronomy systems are using or plan to use optical fibre data transmission [1][2][3]. This improvement for European VLBI can be phased as follows :

- Replacement of the Jodrell Bank to Cambridge microwave link with an optical fibre connection. This will allow the Jodrell / Cambridge telescopes to record VLBI data at the same rate as telescopes elsewhere in the network. Previously, the data rate has been limited to 112Mbps by the bandwidth restriction imposed by the microwave link between the two sites.

- Installation of an experimental optical fibre link between one of the continental European telescopes (e.g Effelsberg) and the correlator at Dwingeloo.
- Full interconnection of the network to the correlator.

If these improvements are to be made, investment should also be planned to upgrade the front end and back end systems e.g bit rate conversion from 2.5Gbps (needed for standard commercial links) to 1Gbps at the correlator, large capacity buffering/storage to cope with throughput of data at the correlator, data to SDH convertor chips etc. .

1.2 General System Outline

Figure 1.1 shows a generalised system architecture for a single optical link from a radio telescope to a correlator site. The signal applied to the optical modulator can be either a wideband IF, defined at the telescope with appropriate down-conversion and filtering or a sampled and digitised version of the IF band.

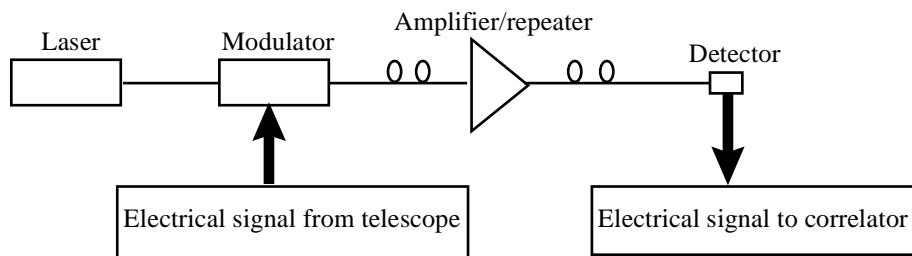


Figure 1.1 Generalised system arrangement for optical link

There are several important system issues that need to be considered in the analysis of such an arrangement :

- *Optical wavelength* - Most installed fibre is designed for use at 1310nm. If long haul links are necessary and multiple wavelength channels are needed then the wavelength must be in the 1550nm region. This will allow optical amplifiers to be used but will also lead to higher chromatic dispersion in the fibre. Single channel links can be implemented with a 1310nm system using electrical repeaters to extend the reach.
- *Digital or analogue* - Analogue modulation avoids the requirement for samplers and digitisers at each telescope site allowing these to be situated at the correlator. Digital systems are much less prone to noise and non-linear effects and so can offer better quality signals over larger distances.
- *Length of link* - This will have an impact on the modulation technique used and the need for mid-span optical amplifiers (or electrical repeaters for single wavelength channels).
- *Data rate* - If a digital implementation is chosen, the data rate will define the maximum instantaneous bandwidth and hence the sensitivity of the radio astronomy measurement. Commercial equipment will require standard data rates to be used (2.5Gbps, 10Gbps) which may not be compatible with the radio astronomy front and back end. It may be necessary to pre-code the data into an SDH

(synchronous digital hierarchy) protocol format acceptable to commercial telecoms equipment (see appendices).

1.3 Structure of the Report

The report covers all aspects of the modelling and definition of optical links for radio astronomy applications and in particular for long haul situations as would be expected within the European VLBI Network. In addition, experimental results are presented where necessary to validate the theoretical modelling. The availability of dark fibre within Europe is also investigated and potential systems architectures are presented with estimated costs. The report is structured as follows :

- Section 2 - Definition of specifications used in the analysis
- Section 3 - Current status of optical components including lasers, modulators, optical amplifiers and detectors. Device characteristics from the major manufacturers are tabulated for comparison.
- Section 4 - Link model development for both analogue and digital modulation including definition of device and system models.
- Section 5 - Analysis of the performance of analogue optical links
- Section 6 - Analysis of the performance of digital optical links.
- Section 7 - Experimental validation of theoretical models.
- Section 8 - Performance and costs of a single link example
- Section 9 - Options for implementation of long haul fibre links
- Section 10 - Conclusions of the study.

1.4 Acknowledgements

The authors would like to thank the following: Dr Lucia Hu for her work on analogue transmission, Drs Dave Moodie, Graeme Maxwell and Mike Robertson of BT Laboratories, Martlesham for their support and donation of equipment under a PPARC funded collaborative research scheme, and finally Drs Patrick Grant and Colin Wallace of Corning Cable Systems for the data on installed fibres in the UK and Europe.

2. SPECIFICATION AND DEFINITION OF PARAMETERS

2.1 System specifications

No definitive system specification has been made available and as a consequence, the following has been assumed to allow system modelling and analysis. For the analogue system, the dynamic range is defined as the difference in power (dB) between the highest RF power (to meet the signal-to-spurious ratio) and the lowest RF power (to meet the minimum SNR requirements). Figure 2.1 shows a schematic of the points defining the dynamic range of the system

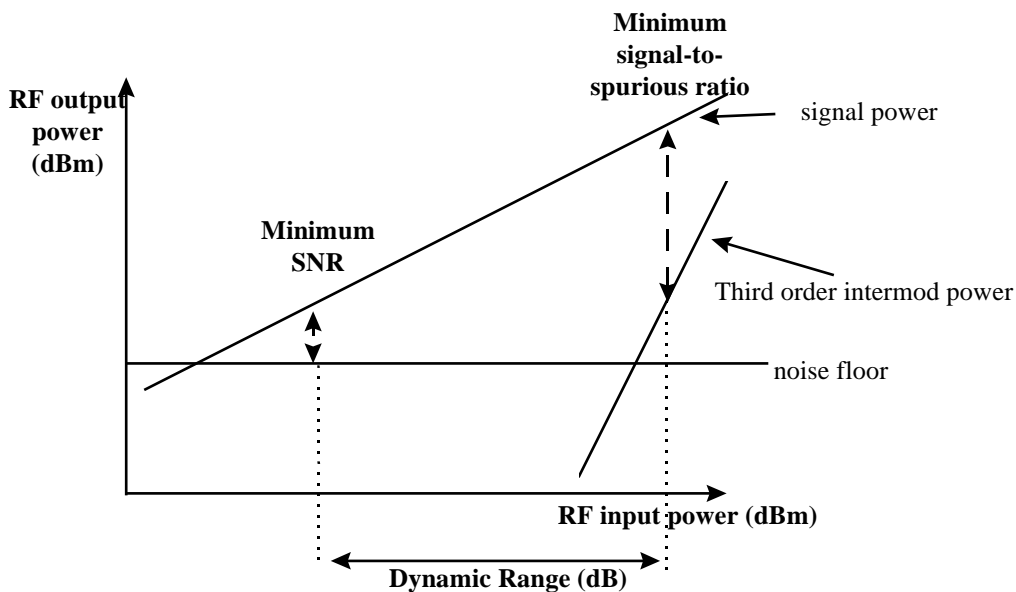


Figure 2.1 Parameter definition for analogue system models

Path Length

Maximum system path length = 3000km

Analogue system

Minimum SNR = 20dB

Minimum signal-to-spurious ratio = 40dB

Bit resolution at correlator = 2 bits (equivalent to a dynamic range of 14dB)

Digital system

Minimum SNR = 20dB

Equivalent minimum bit error rate (BER) = 10^{-5}

3. CURRENT STATUS OF OPTICAL COMPONENTS

3.1 Lasers

There are three types of laser source available suitable for optical fibre systems, namely solid state lasers, semiconductor lasers and fibre lasers. The first of these types, the solid state laser, is generally crystal based, requires a diode laser for pumping and can provide high output powers (100mW), low Relative Intensity Noise -RIN (-170dB/Hz) values and narrow linewidth (<100KHz). The disadvantage is that they are only generally available at a wavelength of 1300nm, tend to be bulky and their optical powers are such that they are likely to cause non-linear effects such as stimulated Brillouin scattering (SBS). Semiconductor lasers on the other hand consist of a forward biased p-n junction formed in a direct band-gap semiconductor material. They exhibit optical powers up to 60mW (18dBm) into fibre, with RIN values better than -160dB/Hz (although this depends on the laser structure used) and linewidths better than 10MHz. Fibre lasers are based on Erbium Doped Fibre Amplifiers, consisting of a loop of rare earth doped fibre, pumped by a laser diode (at 980nm or 1450nm). These devices form a resonant cavity within the fibre loop and so variations in environmental conditions can cause mode hopping (wavelength shifting). To avoid this, the devices tend to be rather bulky and so will not be considered any further in this discussion.

The basic structure for a semiconductor laser described above is referred to as a *homojunction* laser. The p-n junction consists of the same semiconductor material on both sides. Lasing can only be achieved in a pulsed mode and threshold currents are in the range of a few amperes to 10s of amperes. Present day laser diodes have a *double heterostructure* configuration where a thin layer of low band-gap semiconductor is sandwiched between two layers of higher band-gap material. This allows 'carrier confinement' in the junction and hence lower threshold currents. Furthermore, optical energy is confined to the low band-gap material since it has a higher refractive index than the surrounding semiconductor leading to more efficient fibre pigtailed.

The output optical power of a laser diode is dependent on the current passing through the device. A threshold current exists below which the optical power is low. As the current is increased above the threshold, the optical power increases significantly. The optical emission appearing below threshold is mainly due to *spontaneous emission*, whereas above the threshold value it is primarily due to *stimulated emission*. Figure 3.1 Shows a typical current-optical power transfer characteristic with the threshold current at ~65mA.

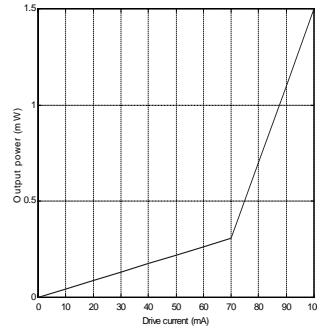


Figure 3.1 Optical power as a function of drive current for a laser diode.

When the current is below the threshold, the laser diode behaves like an LED and the output is mainly due to spontaneous emission (broad spectrum in Figure 3.2(a)). As the current increases beyond the threshold, the frequencies having a larger gain and a lower cavity loss, begin to oscillate and the spectrum changes significantly (multiple modes of oscillation) as shown in Figure 3.2(b).

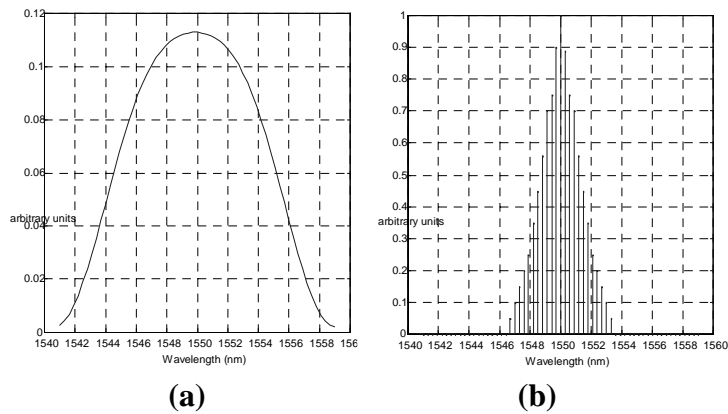


Figure 3.2 (a) Broad output spectrum below threshold **(b)** Multi-longitudinal modes of oscillation generated above threshold current

Figure 3.2(b) shows that a laser diode generally oscillates simultaneously at a number of frequencies giving a spectral response at a range of wavelengths. This type of response is typical for a *Fabry-Perot* cavity laser diode. A frequency spread such as this would lead to potential pulse dispersion degradation in a fibre optic communication system. In addition the achievable RIN for such a device is only $\sim 120\text{dB/Hz}$. To improve the situation, we must use a laser which has only a single mode of oscillation. This is achieved by introducing components into the laser cavity that result in a high loss for all modes of oscillation except one. Techniques involve integrating a Bragg grating filter into the optical cavity resulting in a *distributed feedback* structure (DFB). DFB lasers have significantly narrower linewidth than their Fabry Perot counterparts and are capable of achieving RIN values better than -160dB/Hz .

A selection of lasers available from the major manufacturers is shown in Tables 3.1 and 3.2 below. These are specifically CW lasers for externally modulated analogue and digital systems. It is advantageous if the device is pigtailed with polarisation

maintaining fibre for compatibility with the input fibre pigtail of the external modulator. Most of the manufacturers produce DFB lasers for direct modulation up to 2.5Gbps. Since direct laser modulation introduces dispersion limitations, it is not considered as a feasible option for this application.

Manufacturer	Linewidth (MHz)	Power (dBm)	λ (nm)	RIN dB/Hz	Cooled?	PM fibre?
ORTEL	3	14,15,16	1550	-162	Yes	Yes
ALCATEL	1	17	1550	-	Yes	No
LUCENT	1	5-13	1550	-	-	Yes
NORTEL	<10	3	1550	-	Yes	Yes
NEL	<10	12	1550	-	-	Yes
NEL	<10	3-15	1550	-	-	No
UNIPHASE	<2	13-18	1550	-160	Yes	Yes

Table 3.1 CW lasers for analogue optical link applications

Manufacturer	Linewidth (MHz)	Power (dBm)	λ (nm)	PM fibre?
LUCENT	2-10	10	1530-1563	Yes
UNIPHASE	<5MHz	4, 10, 13	1530-1563	Yes
NORTEL	<10	3	1550	Yes
ALCATEL	<5	10-15	1550	Yes

Table 3.2 CW lasers for digital/analogue link applications

3.2 Modulators

Mach Zehnder Amplitude Modulators

Lithium niobate modulators are based on the Pockels effect which induces a variation of the optical index of the material with the applied voltage. Most of them use the Mach-Zehnder interferometer configuration (see Figure 3.3) in which the change of index in one arm (or both arms with push-pull drive) leads to a variation of the amplitude of the output due to constructive or destructive interference. This technology is now rather mature and so there are a range of component manufacturers. A selection of commercially available 2.5Gbps 10Gbps and 20GHz modulators are listed in the table below. In the research laboratories, the emphasis is essentially on increasing the frequency coverage (cut-off frequencies over 40 GHz have been obtained) and reducing the V_{π} which correspond to the voltage required to go from the minimum to the maximum attenuation.

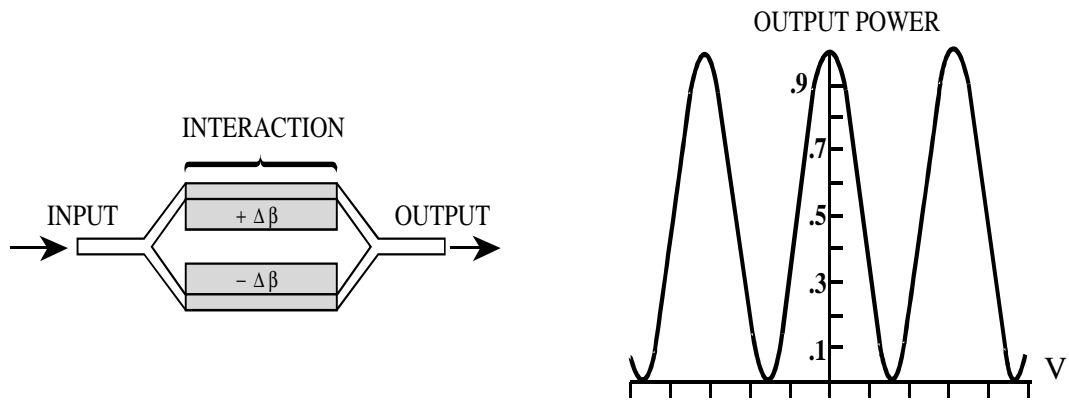


Figure 3.3 The Mach-Zehnder modulator and its transfer function

For applications requiring high levels of optoelectronic integration, Mach Zehnder devices have been developed on GaAs substrates also. There is no difference in the mode of operation compared to those in LiNbO₃ but the GaAs devices suffer from higher optical losses as a result of the mode size mismatch between the integrated optical waveguide and fibre pigtails.

Both Lithium Niobate and Gallium Arsenide amplitude modulators are based on a travelling wave configuration in order to maximise the interaction between the electrical field and optical wave. This means that they can be quite large (cms) requiring significant board space to accommodate the device and the fibre pigtail (at the specified fibre bend radius). Table 3.3 shows the manufacturers of discrete components and their characteristics. To ensure that the modulators perform within specification over time, it is essential that some form of bias control circuitry is implemented to avoid the problems associated with a drifting quadrature bias point. This may consist of detecting a fed-back portion of the output signal and adjusting the bias accordingly (problematic since it is difficult to distinguish between varying laser power and varying bias point). Alternatively, manufacturers (eg RAMAR Corp) provide control units based on injection of a pilot tone which are much more efficient than the simple method but significantly more expensive.

Electro-Absorption Modulators

EAMs are semiconductor devices which are usually implemented in materials containing indium, gallium or aluminium with either phosphorus or arsenic. They are buried heterostructure devices (Figure 3.4) with an optically guiding absorber region located between a p-doped and n-doped region. The absorber region usually consists of multiple layers of suitable band-gap material in the form of a multiple quantum well (MQW).

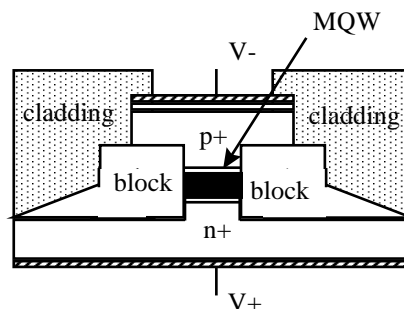


Figure 3.4 EAM modulator cross section

The optical signal travels in the MQW region. The optical properties of the region can be altered by applying an electric field between the contacts across the p-n junction providing an 'on' state allowing the signal to pass through and an 'off' state in which the absorption is high, causing attenuation. These devices tend to be offered as integrated transmitter units (see section 3.3) and are not often available as stand-alone devices at the moment. Electro-absorption modulators have advantages over Mach Zehnder devices in terms of size, level of component integration and extinction ratio (30-40dB compared to 15dB for MZ) but insertion loss is sensitive to both bias voltage and wavelength.

Manufacturer	Loss (dB)	Vπ (volts)	Bandwidth (GHz)	Return Loss elec (dB)
LUCENT	3 - 6.5	<4.5	10	-15
JDS	4	3 - 10	1,3,10,12	-20
SUMITOMO	<5	<5.5	5, 10, 20, 40	-
RAMAR	4.7	9	20	-10
SDL	2.5 - 5	8	2.5, 10	-8

Table 3.3 Lithium Niobate MZ amplitude modulators

3.3 Integrated Transmitters

Where space is at a premium or if interconnect complexity is to be minimised, some manufacturers produce integrated transmitter units which consist of a DFB laser co-packaged with an amplitude modulator. Most of the devices available consist of DFB lasers and EAM devices in a single package however NORTEL supply a packaged DFB and LiNbO₃ modulator for operation up to 10GHz whilst Marconi supply integrated DFB, GaAs modulator chips up to 40GHz. Some of the available devices are described in Table 3.4

Manufacturer	Power (dBm)	λ (nm)	Bandwidth (GHz)	Modulator
NORTEL	0	1557	10	LiNbO MZ
	1 - 5	1550	2.5	"
NEL	3	1550	10	EAM
LUCENT	1	1550	2.5, 10	EAM
ALCATEL	0	1550	2.5	EAM
MARCONI	-	1310, 1550	<40	GaAs MZ
ERICSSON	-2	1550	12	EAM

Table 3.4 Co-packaged laser diodes and modulators

3.4 Photodiodes

PIN photodiodes (Table 3.5)

The most common semiconductor photodetector is the PIN photodiode, which consists of a lightly doped semiconductor sandwiched between a p-doped and an n-

doped region. The PIN photodiode is normally subjected to a reverse bias and since the lightly doped 'i' region has no free charges, most of the voltage exists across this part of the device. The electric field in the 'i' region is high and so any photo-generated e-h pairs are immediately swept away by the field resulting in a photocurrent.. The 'i' layer of these devices is usually large to ensure that most photons are absorbed in this region. This results in good quantum efficiency and hence good responsivity (photocurrent generated per unit optical power in A/W). The width of the intrinsic region cannot be made too large since the carriers would then take longer to drift to the terminals and thus reduce the speed of response (bandwidth) of the detector. PIN photodiodes for operation at 1550nm usually consist of Germanium, Indium Phosphide (InP), or InGaAs

APDs (Table 3.6)

An APD (avalanche photodiode) is a device with an internal current gain that is achieved by having a large reverse bias. In the APD, absorption of an incident photon produces an e-h pair as in the PIN device. The large electric field in the depletion region causes the charges to accelerate rapidly such that they can impart enough energy to excite an electron into the conduction band. This results in an additional e-h pair, which in turn can generate more e-h pairs. The process leads to an avalanche multiplication of the carriers and hence current gain. For avalanche multiplication to take place, the diode must be subjected to a large electric field. Compared to PINs where bias voltages of 5-15V are common, APDs typically require voltages of 20-30V.

Manufacturer	Responsivity A/W	Bandwidth GHz	Overload dBm	Sensitivity dBm
ERICSSON	1	2.5	0.5	-25
EPITAXX	0.9	10	0	-17
LASERTRON	0.8	18	5	-
DISCOVERY	<0.7	8 - 50	-	-
ORTEL	0.8	10	2	-20
OCP	-	1.5	2	-26
NEL	<0.8	8 - 50	-5 to 13	-
LUCENT	<0.95	1	0	-
NORTEL	0.8	8	0	-
ALCATEL	- 0.95	3 3	3 9	-21 -

Table 3.5 PIN photodiode modules

Manufacturer	Responsivity A/W	Bandwidth GHz	Overload dBm	Sensitivity dBm
ERICSSON	11.5	2.5	-4	-34
EPITAXX	0.7	10	-7	-23
LUCENT	10.7	3	-	-
NORTEL	-	2.5	-7	-34
ALCATEL	0.95 -	3 3	+6 -5	- -34

Table 3.6 APD photodetector modules

3.5 Optical Interfaces

As well as discrete components, optical/electrical interface modules are also available on the market which operate over the range of SDH/SONET rates. ALCATEL produce a transmitter / receiver pair capable of providing STM1 (155Mbps) up to STM4 (622Mbps). The transmitter unit consists of laser, driver, cooling and monitoring functions in a single unit. Electrical multiplexing (if required) is not supplied in the unit. The receiver operates to a minimum optical power of -28dBm which sets the repeater spacing at around 130km maximum. The receiver unit also contains clock recovery, re-timing and data monitoring functions. JDS-Uniphase supply a similar unit capable of rates up to 10Gbps which can be supplied with electrical multiplexing from STM1 to STM4. The receiver has integrated clock and data recovery circuitry. ERICSSON also manufacture a transmitter / receiver pair for data rates up to 2.5Gbps, single channel and WDM.

3.6 Optical amplifiers

The aim of an optical amplifier is to provide gain for the input optical signal, without optical to electrical and electrical to optical conversions. This type of amplifier is transparent to the modulation signal (analogue or digital, frequency or bit rate). There are two types of optical amplifier available: the doped optical fibre amplifier (DFA) and the semiconductor optical amplifier (SOA). They both operate on the same principle of energy absorption and stimulated emission, but they differ in the active material used (rare earth ions and semiconductor) and in the way they are pumped (optically and electrically respectively).

A schematic of a DFA is shown in Figure 3.5. It comprises a section of rare earth doped fibre. Pump light is generally produced by a semiconductor laser diode and is coupled into the active fibre using a wavelength division multiplexer (WDM). Optical isolators are used to prevent optical reflections and laser oscillation. The diagram shows the co-propagation configuration of the amplifier. Counter-propagation exists when the pump light is launched in the opposite direction to the signal.

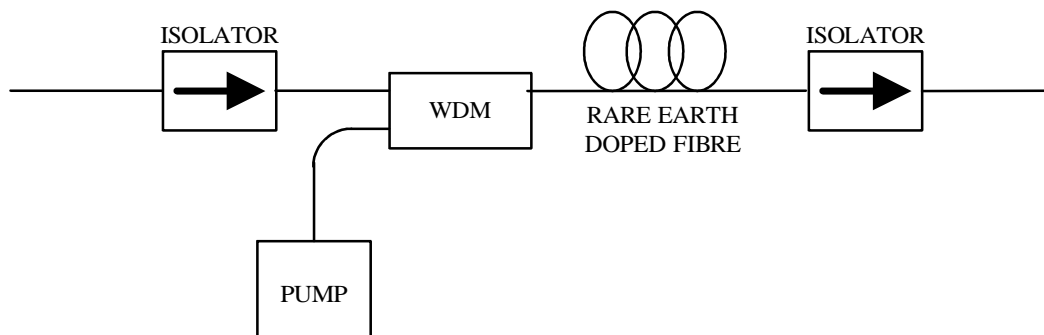


Figure 3.5 Doped optical fibre amplifier scheme

The DFA is inherently compatible with optical fibre transmission. There are coupling losses due to splicing and passive optical components (isolators, WDM, etc) but this can be limited to less than 2 dB.

One feature of a DFA is that the optical gain is dependent on the input signal level. For small optical input powers (less than 1mW) the optical gain is a constant maximum. As the input power increases, the gain decreases and the amplifier eventually saturates. The saturation optical power can be as high as +27 dBm for erbium doped fibre at 1.55 μm . Typical figures for an EDFA, with standard pump diodes, are +15 dBm saturated output power and 30 dB of gain (Figure 3.6).

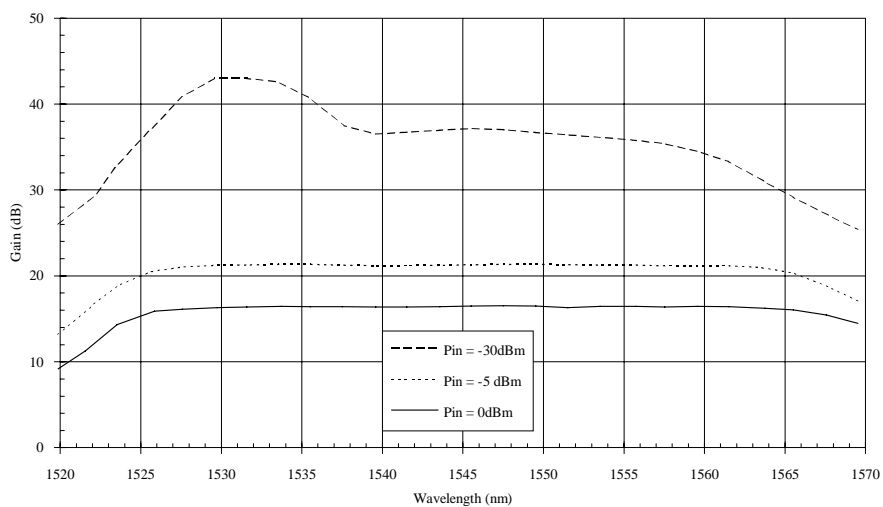


Figure 3.6 Gain-wavelength characteristics for various input powers

One interesting EDFA characteristic is the high linearity of the amplifier even in the gain compression regime. This is due to the long time constants (around 10 ms for erbium) for excitation and relaxation of the rare-earth ions. This results in an amplifier gain which is slow to respond to changes in the level of the pump or the input signal. The instantaneous amplifier gain is independent of signal format (assuming a frequency modulation greater than a few tens of kHz for erbium) even when the amplifier works deep into saturation at the maximum output power. This means that when many different signal wavelengths are present, the effect of crosstalk and intermodulation products is negligible.

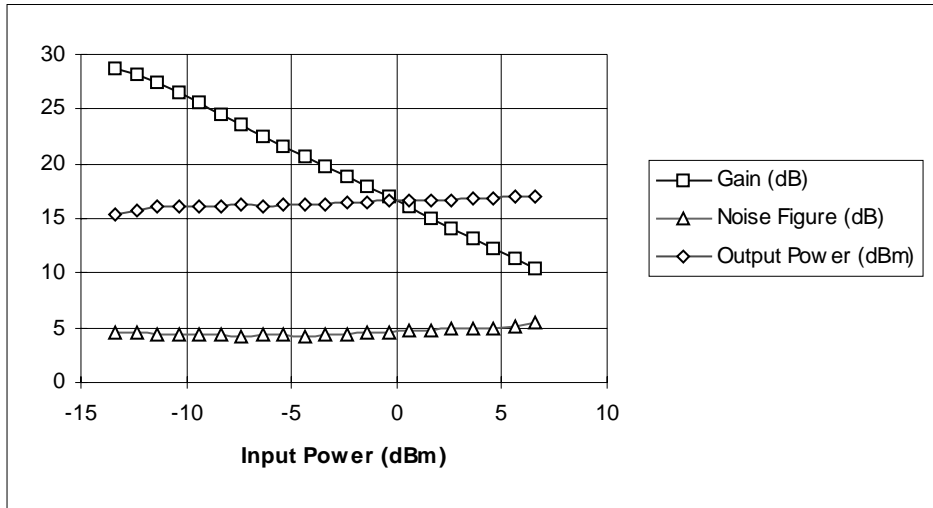


Figure 3.7 Characteristic curves for Ericsson +16dBm EDFA

The characteristics of a typical EDFA are shown in Figure 3.7. The diagram shows the region close to saturation, where the gain reduces with input optical power to maintain a constant output power. It is clear that for this amplifier, the noise figure is independent of input optical power. Data from the above characteristic is used in the link modelling to ensure that the calculations take account of the typical gain saturation performance of optical amplifiers.

Manufacturer	Gain (dB)	Psat (dBm)	Noise Figure (dB)	Features
Nortel	<30	13 - 18	<5	
Alcatel	-	10 - 16	~7	
NEL	17 - 38	12 - 19	5 - 7	
Ericsson	30	16, 19	<6dB	
JDS Uniphase	-	<17	-	mid stage access
Highwave	30	10 - 15	4.5	preamp in-line booster
	25	14 - 22	5	
	15	14 - 22	6	
Optigain	-	10 - 21	-	compact
IRE-polus	-	13 - 40	-	high power

Table 3.7 Characteristics of some currently available EDFAs

4. OPTICAL LINK MODEL DEVELOPMENT

4.1 Analogue Optical Links

The following section will introduce the definitions and conventions used in the modelling of RF optical links based on a simple point-to-point externally modulated optical link. The evolution of signal power through the link will be discussed and sources of noise will be presented including those arising from single and cascaded optical amplifiers. The model will be further extended to define the gain, noise figure and third order intercept point (TOI). In addition, an analysis of the effects of dispersion in long-haul analogue optical links will be discussed and a model presented. The effect of non-linear phenomena such as stimulated Brillouin scattering (SBS) will be considered.

4.1.1 System Definitions

Figure 4.1 shows a simple analogue optical link including RF pre-amplification and post detection amplification. The optical link can be considered as an RF component with gain (G_2), a certain noise figure (F_2) and a third order intercept point (TOI2). To achieve the required specification (gain, SNR and dynamic range) it is likely that RF pre-amplification and/or post detection amplification will be required. These components will contribute to the overall link gain, link noise figure and link TOI.

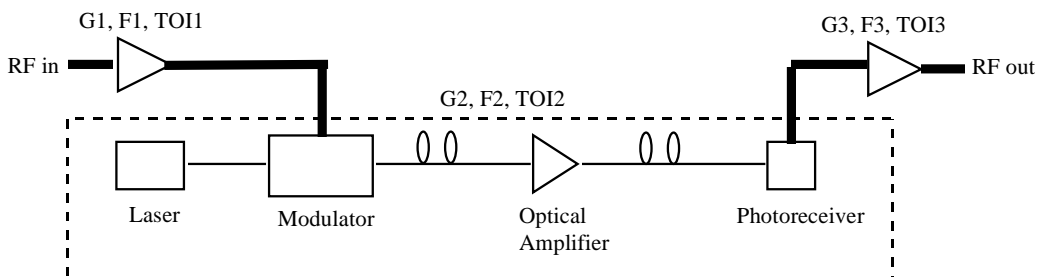


Figure 4.1 Simple point-to-point optical link with pre and post RF amplification

Using the above representation, the component characteristics can be combined to evaluate the total link characteristic. It is convenient to represent this type of system using a plot of RF input power against RF output power as shown in Figure 4.2. The plot shows the variation of RF signal power, the total noise power and the effect of third order intermodulation distortion. Second harmonic distortion can arise from microwave amplifiers, but this will be ignored at this point.

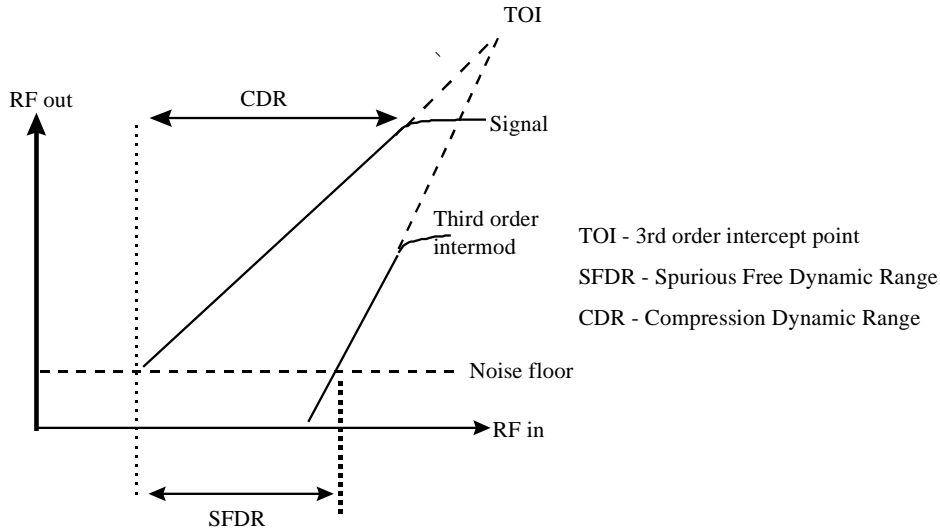


Figure 4.2 Definitions of third order intercept and dynamic range

The above diagram shows the accepted conventions for third order intercept (TOI), spurious free dynamic range (SFDR) and compression dynamic range (CDR). Neither of these measures will be used for radio astronomy performance measurements. The dynamic range is defined by a minimum of 20dB signal-to-noise ratio (see specifications section 2.1), which sets the lowest RF input power achievable and a minimum of 40dB signal-to-spurious (3rd order) which sets the highest RF power.

4.1.2 Evolution of Signal and Noise in Analogue Optical Systems

Considering an intensity modulated direct detection scheme as shown in Figure 4.1, the signal current at the receiver is :

$$\langle i^2 \rangle = P_{rx}^2 \cdot R^2 \cdot \alpha^2$$

where P_{rx} is the received optical power, R is the photodiode responsivity and α is the loss (gain) of the optical link from laser to detector. Noise at the detector output arises from several sources including :

Thermal noise : Thermal noise is generated in resistive elements of the link including the photodiode and the modulator. Its mean square current value is given by :

$$i_{th}^2 = \frac{4 \cdot k \cdot T \cdot B}{R_l}$$

where k is Boltzmann's constant, T the absolute temperature, B is the bandwidth and R_l , the load resistance value.

Shot noise : Shot noise is generated when an optical signal is incident on the photodetector and is given by :

$$i_{sh}^2 = 2e(i + i_d) \cdot B$$

where e is the electronic charge, i is the mean optically generated current and i_d is the photodetector dark current..

Relative Intensity Noise (RIN) : Relative intensity noise is generated by spontaneous emission within the laser source and is dependent on a number of material, structural and modulation parameters. The contribution of the source RIN to the noise current at the detector for a CW laser is given by :

$$i_{RIN}^2 = i^2 RIN . B$$

Typical values of RIN for a distributed feedback (DFB) laser are better than 155dB/Hz.

Assuming that all of these noise sources are uncorrelated, the signal-to-noise ratio at the detector output can be expressed by :

$$SNR = \frac{P_{rx}^2 . R^2 . \alpha^2}{\left(\frac{4kT}{R_i} + 2e(R\alpha P_{rx} + i_d) + (R\alpha P_{rx})^2 . RIN \right) . B + i_{amp}^2}$$

where i_{amp} is the contribution to the noise from optical amplifiers in the link.

Disregarding the optical amplifier noise for the moment, an optical link will generally be 'limited' by the most dominant noise from the above list. The total noise will be the sum of the above components and since some of these components are signal dependent, the limiting noise will be dependent on the received optical power. Figure 4.3 shows how the noise floor varies with varying received optical power.

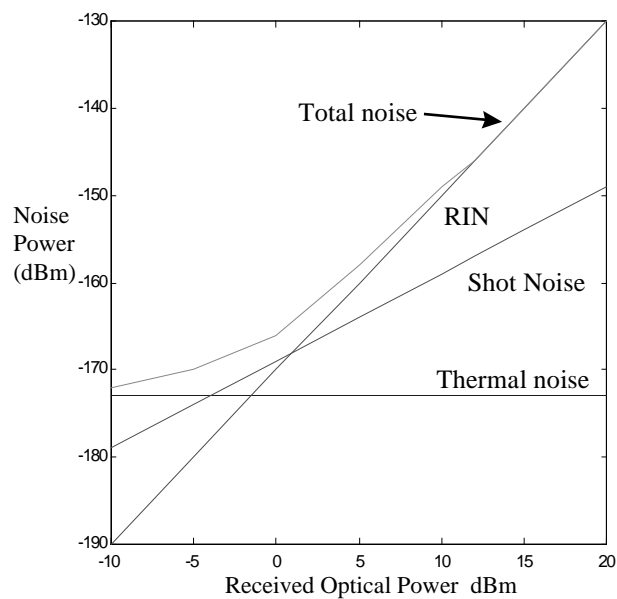


Figure 4.3 Variation of received noise power against received optical power

Figure 4.3 is calculated for a system with a laser RIN of -155dB/Hz. It does not take into account any saturation in the photodetector which would generally occur for received optical powers above 6dBm. There are three distinct regions where the link can be described as :

- Thermally noise limited (for received optical powers below -5dBm). In this region, increasing the optical power transmitted by 1dB will generally improve the signal-to-noise (SNR) ratio at the receiver by ~1dB.
- Shot noise limited (for received optical powers between -5 and 1dBm). In general, if a link is shot noise limited, a 1dB increase in optical power will improve the SNR by 0.5dB.
- RIN limited (received optical powers above 1dBm). If the link is RIN limited there is no benefit in system SNR of increasing the optical power.

4.1.3 Optical Amplifier Noise

For the radio astronomy application, a signal to noise ratio of 20dB is required at the correlator. Since our discussion involves long haul links of up to 3000km, it is clear that the large fibre losses will have to be overcome to maintain the SNR within specification. Figure 4.3 showed that SNR could be improved up to a point (the RIN limit) by increasing the laser power. This technique is unlikely to maintain the required specification over distance and so optical amplifiers will be required.

Section 3.4 discussed the operation of Erbium Doped Fibre Amplifiers (EDFA's). In an amplifier exhibiting population inversion such as an EDFA, there is a natural decay from upper to lower energy states. Such transitions result in the emission of photons unrelated to the signal and it is this spontaneous emission that is the source of noise within the amplifier.

A single optical amplifier will generate an amount of ASE optical power given by [4][5][6]:

$$P_{ase} = \gamma(G - 1).h.v.B_o$$

where G is the amplifier gain, $h\nu$ is the photon energy and B_o is the amplifier optical bandwidth (which can be defined using an optical filter to reduce ASE) and γ is the population inversion factor (for an ideal amplifier $\gamma=1$).

This optical noise power will generate shot noise in the receiver but the power level will be very much less than the mean optical signal power and so the shot noise associated with the ASE can be neglected. In terms of the noise floor that would be seen on a spectrum analyser, the relevant terms are the beat noise terms generated by signal-spontaneous (beating between the main optical carrier and the ASE noise spectrum) and spontaneous-spontaneous (pair-wise beating between all of the various [infinite] combinations of components of the ASE spectrum). The equivalent photocurrents generated by the optical signal and the ASE are given by :

$$I_1 = 2 \cdot e \cdot \eta \cdot P_s \frac{\lambda}{h \cdot c}$$

$$I_{ase} = e \cdot \eta \cdot P_{ase} \cdot \frac{\lambda}{h \cdot c}$$

Here, e is the electronic charge, P_s is the received signal power and η is the quantum efficiency. The mean square electrical noise currents of the beat noise terms are then expressed as [5] :

$$i_{sig-sp}^2 = 2 \cdot I_{ase} \cdot I_1 \cdot \frac{B_e}{B_o}$$

$$i_{sp-sp}^2 = I_{ase}^2 \cdot \frac{B_e}{B_o}$$

B_e is the electrical bandwidth and B_o is the optical bandwidth as above.

Using the above expressions, we can investigate the effect of multiple EDFA's in cascade as would be the case for a long haul optical link. In these situations, the noise from each amplifier is accumulated along the link, reducing the signal to noise ratio at the receiver. Figure 4.4 shows such a system of amplifiers.

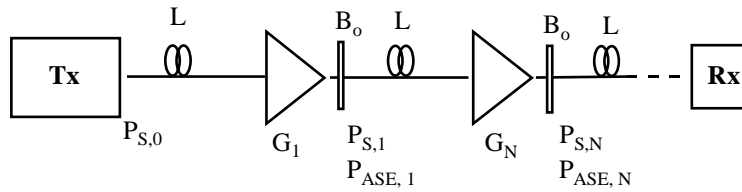


Figure 4.4 Cascade of optical amplifiers

L is the loss associated with each fibre span between amplifiers. An optical filter with bandwidth B_o is used at the output of each amplifier to reduce the effect of the spontaneous-spontaneous beat noise. The evolution of signal and noise along the link can be expressed as :

$$P_{ase,i}^{Tot} = LG_i P_{ase,i-1}^{Tot} + P_{ase,i}$$

$$P_{s,i} = LG_i P_{s,i-1}$$

The above equation ignores the effect of ASE reducing the signal power along the cascade. The result of these recurrence relations can be inserted into the photocurrent expressions and hence the contributions from signal-spontaneous and spontaneous-spontaneous noise from the cascade can be determined.

4.1.4 Optical Amplifier Saturation

We have seen from section 3.3 that as the input power to an optical amplifier increases, the gain reduces to maintain the output power at a level known as the saturation output power. This effect must be taken into account in the modelling to

avoid erroneous calculation of continually increasing optical power levels over amplifier cascades.

The process was modelled using data from a typical optical amplifier manufacturer which detailed the variation of optical gain with input optical power. Additional data was added to specify the saturation dynamics over a larger range of optical powers (from -20dBm to +20dBm). For the gathered data points, an algorithm was developed to calculate the actual gain as a function of the input power and the defined saturation output power and these results were used within MATLAB's polynomial curve fitting routine to estimate a 7th order representation. Figure 4.5 shows results obtained for typical optical amplifier gains and saturation powers. The agreement between the actual and predicted curves is excellent.

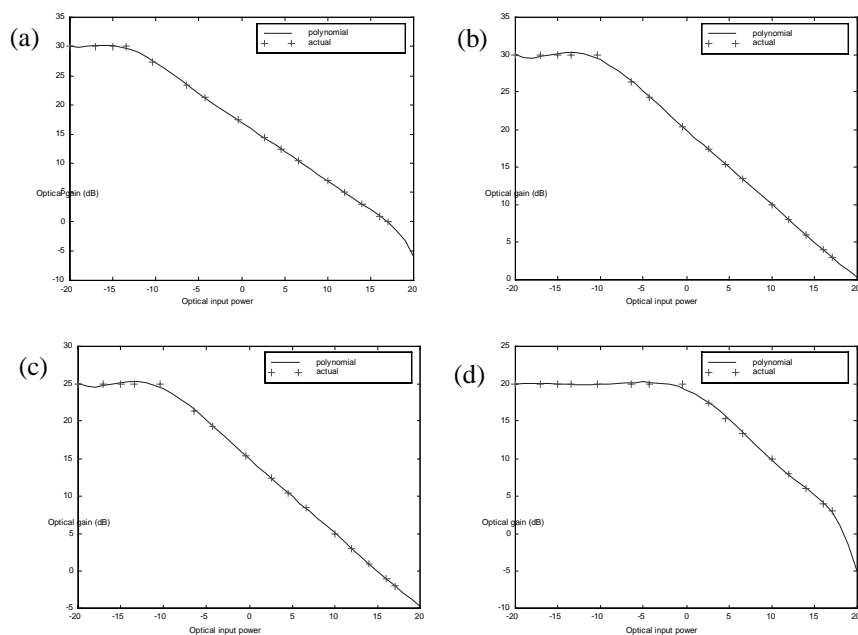


Figure 4.5 Comparison of actual saturation response with polynomial prediction (a) 30dB gain, 17dB sat (b) 30dB gain 20dB sat (c) 25dB gain 15dB sat and (d) 20dB gain ,20dB sat

4.1.5 Determination of Performance Metrics for Analogue Systems

In this work, only externally modulated optical links will be considered. Directly modulated systems are ignored for several reasons. They are inherently more linear than their externally modulated counterparts but unlike externally modulated links, the SNR improvement achievable by increasing the optical power is limited, to avoid saturation of the laser and generation of the associated non-linearities. In addition, directly modulated systems suffer from laser chirping which can make long haul transmission over standard optical fibre practically impossible.

It has been shown [7] that an intensity modulator has a voltage - optical intensity relationship that can be expressed as (see section 3.2):

$$I = I_0 \cos^2\left(\frac{\pi.V}{2.V_\pi} - \frac{\phi}{2}\right)$$

In the expression, I_0 is the input optical power, V is the input voltage to the device, V_π is the voltage required to achieve a π optical phase shift. I is the modulated optical power and ϕ is the static bias phase shift. Using standard trigonometric identities, this expression can be written as :

$$I = \frac{I_0}{2} + \frac{I_0}{2} \cos\left(\frac{\pi.V}{V_\pi} - \phi\right)$$

At quadrature bias, the static phase shift is $\pi/2$ and so ; $\cos(x-\pi/2) = \sin(x)$. Furthermore replacing $\sin(x)$ with its infinite series leads to the expression :

$$I = \frac{I_0}{2} + \frac{I_0.\pi.V}{2.V_\pi} - \frac{I_0.\pi^3.V^3}{6.V_\pi^3}$$

The above equation has a dc term, a linear term and a third order term. This expression will be used to define the third order intermodulation effects when the exciting voltage consists of a two-tone signal. The simplifications above were performed under the assumption that the modulator is biased at quadrature. For this reason the expanded expression is only valid for small voltage incursions around quadrature. Figure 4.6 shows a comparison of the original expression and the simplified expansion around the quadrature point. It is clear from the graph that the expression is only valid for voltages $< 1v$ (peak). This is equivalent to an input RF power of approx 13dBm (assuming a modulator impedance of 26Ω).

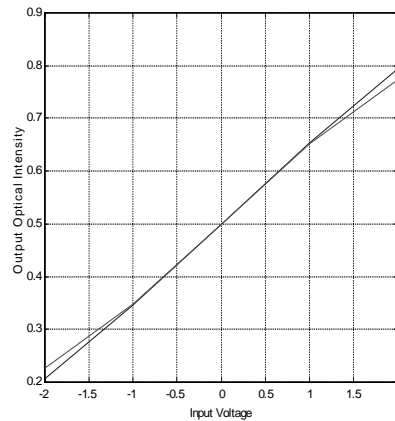


Figure 4.6 Comparison of true modulator transfer function and approximation at quadrature point.

With this in mind, the expression can be used to calculate the signal power and third order intermod product power for various RF input powers as shown in Figure 4.7.

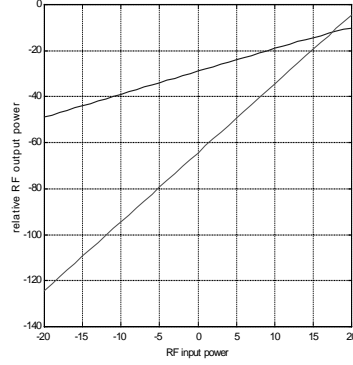


Figure 4.7 Calculation of signal and third order intermod for various RF input powers. For the third order calculation, it has been assumed that both tones at the modulator have the same power

Calculation of Gain

The gain is calculated as the ratio of microwave power received at the detector to the power injected into the amplitude modulator. The input power P_{in} is defined as :

$$P_{in} = \frac{V_m^2}{2 \cdot R_{mod}}$$

where V_m is the peak amplitude of the modulating voltage and R_{mod} is the characteristic impedance of the modulator. The output power P_{out} can be represented by :

$$P_{out} = \frac{I_{ph}^2 \cdot \pi^2 \cdot V^2}{2 \cdot V_\pi^2} \cdot R_{pd}$$

where I_{ph} is the received photocurrent (calculated from the received optical power and the photodiode responsivity). R_{pd} is the load impedance of the photodetector. The gain of the link can then be represented by :

$$G = R_{pd} \cdot I_{ph}^2 \cdot \frac{\pi^2}{V_\pi^2} \cdot R_{mod}$$

Calculation of Noise Figure

The noise figure is defined as the ratio of the input SNR to the output SNR. In terms of link gain this is equivalent to

$$NF = \frac{1}{G} \cdot \frac{N_{out}}{N_{in}}$$

In dB, this can be represented as $NF(\text{dB}) = -G(\text{dB}) + N_{out}(\text{dB}) + N_{in}(\text{dB})$.

The input noise is defined by the thermal noise of the modulator as kTB, where k is Boltzman's constant (1.38×10^{-23}) and T is the temperature in Kelvins (298K).

As previously discussed, the output noise is made up of three components (plus an additional component if an optical amplifier is present), thermal noise, shot noise and RIN. The total noise is given by :

$$N_{out} = k.T.B + R_{pd}.2.e.I_{ph}.B + R_{pd}.RIN.I_{ph}^2.B$$

The above expressions allow the calculation of the total link noise figure including the RF amplification components using Frijs formula as :

$$NF_{link} = 10.\log \left[NF_1 + \frac{NF_2 - 1}{G_1} + \frac{NF_3 - 1}{G_1.G_2} \right]. \text{DB}$$

Calculation of the Third Order Intercept Point

Using the expanded expression for the modulator transfer characteristic and assuming that the input RF signal consists of two tones close in frequency to each other with identical power, the optical system third order intercept (TOI) can be obtained :

$$TOI = \frac{4}{R_{mod}} \cdot \frac{V_{\pi}^2}{\pi^2} \text{ dBm}$$

The total link TOI can then be calculated by referring all of the component TOIs to the input of the system and using the well known equation :

$$TOI_{link} = 10.\log \left[\frac{1}{\frac{1}{TOI_1} + \frac{1}{TOI_2} + \frac{1}{TOI_3}} \right] \text{ dBm}$$

4.1.6 Chromatic Dispersion in Analogue Optical Links

The effects of chromatic dispersion in microwave and millimetre wave optical links has been the subject of increasing interest in the past few years [8][9][10] as a result of the demand for wireless access to broadband network services at frequencies around 30GHz and 60GHz.

In conventional intensity modulation, the optical carrier is modulated to generate an optical field with a carrier and two side-bands (double side-band modulation[DSB]). At the optical receiver, each side-band beats with the optical carrier, generating two beat signals which constructively interfere to produce a single component at the RF frequency. If the signal is transmitted over optical fibre, chromatic dispersion causes each spectral component to experience different phase shifts depending on the path length, modulation frequency and the fibre dispersion parameter. These phase shifts

result in relative phase differences between the carrier and each side-band which results in a power degradation of the composite RF signal. When the phase difference is π , complete cancellation of the RF signal occurs.

It can be shown [8] that phase changes in the optical side-bands alter the resultant phase of the RF beat signals and the RF power of the generated radio frequency will vary approximately as :

$$P_{rf} \propto \cos\left[\frac{\pi.L.D}{c}\lambda^2.f_{rf}\right]$$

where D is the dispersion parameter of the fibre (ps/nm.km), L is the length of the fibre and λ is the wavelength of the optical carrier.

The effects of chromatic dispersion with varying path length and frequency can be determined using this expression. Figure 4.6 shows the effect of dispersion on achievable bandwidth for a path length of 50km and a fibre dispersion of 17 ps/nm.km. The diagram shows only the dispersion penalty and does not include the losses introduced by the modulator or fibre link.

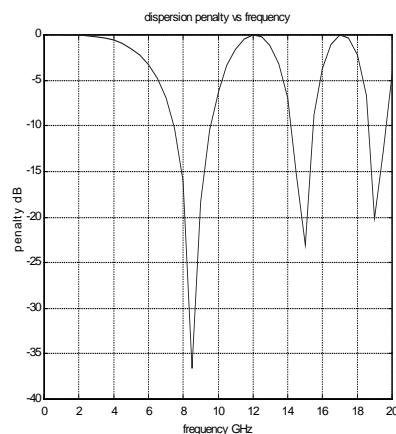


Figure 4.8. Dispersion penalty as a function of RF frequency

Reducing the length of the fibre from 50km to 10km increases the available 3dB bandwidth from ~6GHz to ~13GHz as shown in Figure 4.9.

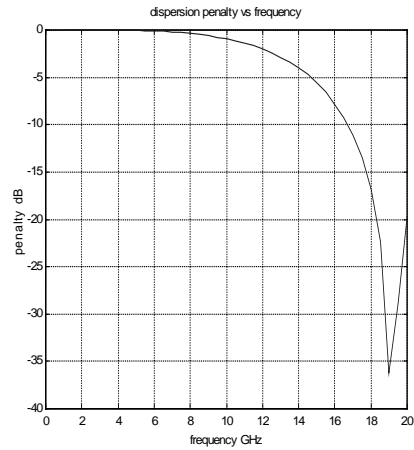


Figure 4.9. Dispersion penalty for 10km link

It is possible to determine the effect of chromatic dispersion on fibre length as shown in Figure 4.10, for a fixed frequency of 10GHz. It is clear that the path length in this case is dispersion limited to less than 20km (assuming that the aim is to accept a maximum dispersion penalty of 1-3dB in the link).

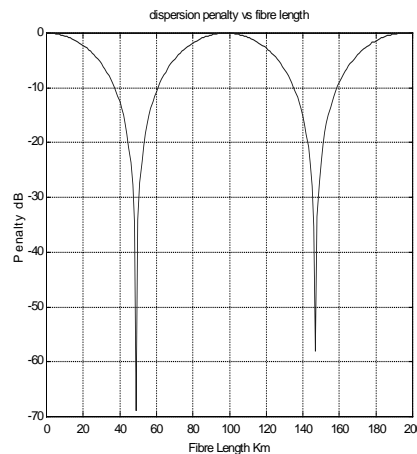


Figure 4.10. Effect of dispersion penalty on fibre path length

4.1.7 Effects of Stimulated Brillouin Scattering on Analogue Optical Systems

One of the great advantages of using an externally modulated link for an analogue transmission system is that for most applications, they are either shot noise or thermally noise limited. As a consequence of this, the signal-to-noise ratio achieved can be improved upon by simply increasing the optical power of the laser. The increase in market demand for high power lasers within CATV transmission systems has led to the availability of DFB lasers at 1550nm with launched fibre powers up to 60mW (18dBm) and RIN values better than -160dB/Hz. Solid state lasers are also available up to 100mW power levels offering RIN figures better than -170 dB/Hz and linewidths better than 100KHz.

The flaw in this scenario is that non-linear effects in optical fibres make it impossible (or at least very difficult) to make effective use of high transmitter power. The most important effect for a single wavelength analogue optical system is stimulated Brillouin scattering (SBS) [11][12][13].

SBS is a non-linear effect caused by acoustic vibration in the fibre, leading to back scattering of the signal and subsequent reduction in signal-to-noise ratio. The level of back scattering is dependent on the incident power in the fibre. The threshold power below which there is less than 1dB signal-to-noise degradation for externally modulated systems is given by :

$$P_{th} = \frac{21.A.\alpha}{\gamma.(1 - e^{-\alpha.L})}$$

P_{th} is the threshold power in watts, A is the core area in cm^2 , α is the fibre loss in cm^{-1} .

γ is the Brillouin gain coefficient in cm/w which is given by [11] :

$$\gamma = \frac{1.73 \times 10^{-10}}{\lambda^2 \cdot \Delta\nu} \text{ cm/w}$$

In this expression, λ is the wavelength in μm of the optical signal and $\Delta\nu$ is the linewidth in GHz.

As an example, consider a laser with a wavelength of 1550nm and a linewidth of 5MHz (typical of a CW DFB laser). Assuming a typical single mode fibre with core diameter 9 μm , a fibre loss of 0.2dB/km and a fibre length of 200km, the threshold optical power for a SNR penalty less than 1dB is 9dBm. This is the threshold power launched into a fibre and so if we take into account the loss in the modulator (~7.7dB at quadrature), we can use a laser power up to ~17dBm (50mW) before SBS will have a significant effect.

4.2 Digital Optical Links

Digital communications systems have many advantages over analogue systems brought about by the need to detect only the presence or absence of a pulse rather than measure the absolute pulse shape. Such a decision can be made with reasonable accuracy even if the pulses are distorted and noisy. For single wavelength systems, repeaters allow new clean pulses to be generated if required, preventing the accumulation of distortion and noise along the path.

4.2.1 Signal Formats

In optical communications systems, the pulse sequence is formed by turning on and off an optical source either directly or using an external modulator. The presence of a light pulse would correspond to a binary 1 and the absence to a binary 0. The two commonly used techniques for representing the digital pulse train are non return to zero (NRZ) and return to zero (RZ). In the case of NRZ, the duration of each pulse is

equal to twice the duration of the equivalent RZ pulse. The choice of scheme depends on several factors such as synchronisation, drift etc. An ac coupled photoreceiver will generally not pass a signal with long sequences of '1's or '0's and so some form of RZ coding scheme would be required.. One frequently used coding scheme is 'Manchester Coding' as shown in Figure 4.11.

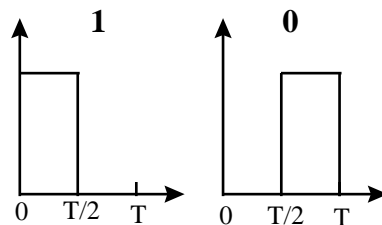


Figure 4.11 Representation of pulses in Manchester Encoding scheme

4.2.2 Noise in Detection Processes

Thermal noise

As we have seen, this arises in the load resistor of the photodiode circuit due to random thermal motion of electrons. This motion leads to the presence of a random current in the resistor. The mean square thermal noise current in a load resistor R_L is given by :

$$i_{th}^2 = \frac{4.k.T.\Delta f}{R_L}$$

The bandwidth Δf is equivalent to the bit rate for RZ (return to zero) coded signals and (0.5x bit rate) for NRZ (non return to zero) signals.

Shot noise

Shot noise arises from the random generation of electron-hole pairs within a photodetector (or any p-n junction device). Even if a photodiode is illuminated with a constant optical power P , the current will fluctuate around an average value determined by the average optical power. In the absence of any optical power, all photodiodes generate a dark current arising from thermally generated carriers. The total shot noise generated in the device is then :

$$i_{sh}^2 = 2.e(I + I_d)\Delta f$$

Assuming that the detector is a PIN photodiode, with a responsivity R and an incident average optical power of P , then the SNR in this case is given by :

$$SNR = \frac{R^2 \cdot P^2}{2 \cdot e \cdot (I + I_d) \Delta f + \frac{4 \cdot k \cdot T \cdot \Delta f}{R_L} + i_{na}}$$

The terms are as before and i_{na} is the mean square noise contribution from any optical amplifiers in the link.

Avalanche photodiodes on the other hand have gain M . As an example of the effect of each device on the SNR, consider first a silicon PIN photodiode with $R=0.65$ A/W, $i_d=1$ nA and $R_L=1000\Omega$ @ 850nm. For an incident optical power of 500nW and a bandwidth of 100MHz, the signal current is 0.325μA. The mean square shot noise current generated is 3.23nA and the thermal noise contribution is 40.6nA. The system is therefore thermally noise limited and so SNR=18dB.

On the other hand APDs have internal gain due to the avalanche process. In this case the signal current is given by $I=MRP$, where M is the internal gain. The thermal noise generated in this device is identical to that in a PIN photodiode. Shot noise in an APD is given by :

$$i_{sh}^2 = M^{2+x} \cdot 2 \cdot e \cdot (RP + I_d) \cdot \Delta f$$

where x is the excess noise factor which is typically $x=0.3$ for silicon photodetectors and $x=0.7$ for InGaAs devices. With this in mind and with $M=50$ the signal to noise ratio for the equivalent APD device is 34.9dB. This is an improvement of around 17dB over the PIN diode case. If M becomes large and the system becomes shot noise limited then the SNR for an APD device can be worse than the equivalent PIN by a factor of M^x . In the case where a system is severely attenuation limited, or available laser powers and amplifier gains are limited, then the APD device is a useful consideration.

4.2.3 Bit Error Rate (BER)

A regenerator or receiver samples the incoming optical pulses at a rate equal to the bit rate of transmission and a decision is made whether each pulse corresponds to a '1' or '0'. The decision is usually performed by setting a threshold level and any signal above this is taken as '1' whilst any signal below is taken as '0'.

If there is insufficient optical power in the received optical pulses (due to attenuation in the link) or if there has been a large dispersion, there could be errors in the received pulse stream.

In retrieving the information at the receiver, it is necessary that the incoming pulses are sampled at the correct rate. Thus the decision points must remain in correct phase with respect to the pulse train. The clock pulses necessary for the decision operation

are usually derived from the received pulse train itself and so it is essential that there is enough energy content at the frequency corresponding to the bit rate. For this reason long trains of '1's and '0's are not advisable unless an adequate coding technique has been used prior to transmission to ensure that the pulse stream is 'balanced'.

The quality of a digital communication system is specified by its BER which is defined as :

$$BER = \frac{\text{bits.read.erroneously.in.duration.}\tau}{\text{total.number.of.bits.received.in.}\tau}$$

The BER essentially specifies the average probability of incorrect bit identification. In general, the higher the received SNR the lower the BER probability will be. For most PIN receivers, the noise is generally thermally limited, which is independent of signal current. Thus the noise in bit '1' and bit '0' is the same and in such a case, the optimum threshold value setting is at the midpoint of the one and zero levels. Under these circumstances, the BER is related to the SNR by :

$$BER = \frac{1}{2} \cdot \left[1 - \operatorname{erf} \left(\frac{\sqrt{SNR}}{2\sqrt{2}} \right) \right]$$

where erf represents the error function. For SNRs ≥ 16 (~12dB), the BER can be approximated by :

$$BER \approx \left(\frac{2}{\pi \cdot SNR} \right)^{1/2} \cdot \exp \left(\frac{-SNR}{8} \right)$$

Figure 4.12 shows the dependence of BER on SNR as given by the two above expressions showing convergence above SNR's of ~12dB.

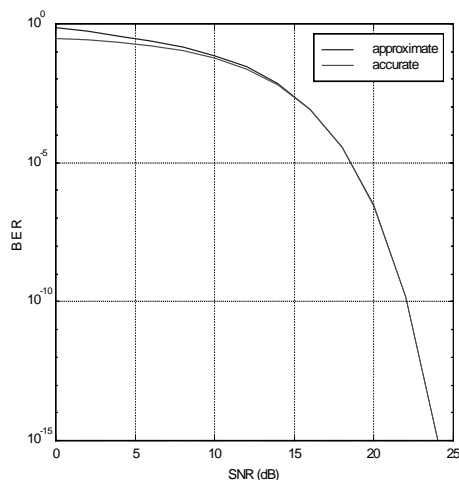


Figure 4.12 Dependence of BER on signal SNR(dB)

4.2.4 Performance of Optical Amplifiers in Digital Optical Links

The expressions for the noise generated by single and cascaded optical amplifiers within a digital optical link are exactly as were developed in Section 4.1.3. The signal-spontaneous and spontaneous-spontaneous mean square noise contributions are added to the thermal and shot noise in the same manner as for the analogue case. This leads to a figure for SNR based on the average received signal power (i.e the average power received assuming a balanced pulse stream of '1's and '0's.) leading to the calculation of BER using the above expressions.

4.2.5 Example Optical Link without Optical Amplification

The following example link is included to introduce the important system parameters from a component selection point of view. Figure 4.13 shows a typical point-to-point digital optical link consisting of a transmitter module, fibre link and a receiver module. The transmitter module is specified by output optical power and wavelength. The receiver module usually has a specified 'receiver sensitivity', which is the minimum power received for a quoted bit error rate (usually 10^{-9}) at a quoted wavelength. The receiver sensitivity is degraded as the data rate increases (more power is required to maintain the same error rate). Usually receiver modules also have a saturated power limit (typically 0dB), above which the unit produces errors.

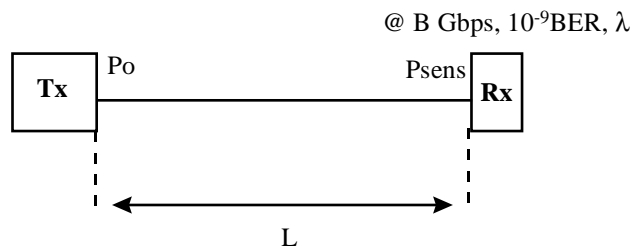


Figure 4.13 Simple digital optical link

Let us assume that the output power of the transmitter module is 0dBm and that the sensitivity of the receiver at 1Gbps is -26dBm. As the data rate is increased, the receiver sensitivity to maintain a BER of 10^{-9} degrades as is shown in Figure 4.14.

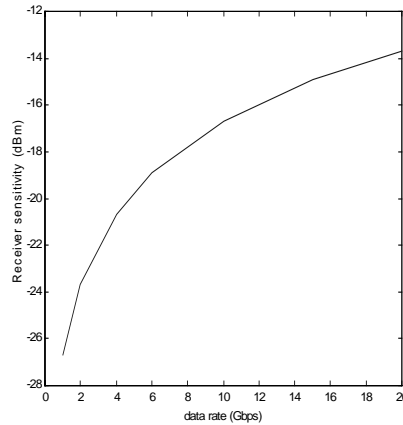


Figure 4.14 Degradation in receiver sensitivity with increasing data rate.

4.2.6 Modelling Chromatic Dispersion in Digital Optical Links

Much of the currently embedded optical fibre was originally designed for light with a wavelength of 1310nm. If this fibre is to be used in optically amplified, high speed and long haul communication systems operating at 1550nm, the chromatic dispersion effects must be taken into account.

Chromatic dispersion is caused by a variation in group velocity in a fibre with changes in optical frequency. If we consider a set of pulses generated by a laser which by virtue of the laser linewidth and signal modulation contains a spectrum of wavelengths. As it traverses the fibre, the shorter wavelength components travel faster than the longer wavelength components and as a result, each pulse experiences broadening. By the time the pulses reach the receiver, they may have broadened over several bit periods and be a source of errors (inter symbol interference). The measure of chromatic dispersion is D , in units of ps/nm/km, which is the amount of broadening in picoseconds that would occur in a pulse with a bandwidth of 1nm while propagating through 1km of fibre. Conventional fibre contains a step index waveguide with a zero in the dispersion near 1310nm. In the 1550nm window, D is approximately 17ps/nm/km.

Dispersion places a limit on the maximum distance a signal can be transmitted. Considering a directly modulated case, at multi gigabit rates the chirp imparted on a laser by modulation is typically 0.5nm (60-80GHz). At 2.5Gbps over conventional fibre the dispersion limited distance is approximately 47km. To significantly increase the span length, one must turn to low-chirp modulation of the optical signal. This can be achieved using an external amplitude modulator. For an externally modulated optical system operating at 1550nm over conventional fibre, the estimated dispersion limited distance is around 1000km at 2.5Gbps. To increase this span length further would require a reduction in the dispersion of the fibre. Currently, there are overwhelming advantages to using erbium doped fibre amplifiers in the 1550nm window to account for attenuation so it is unlikely that systems will revert to 1310nm wavelengths. It is possible to use dispersion shifted fibre (DSF) but much of the

installed trunk network is exclusively conventional fibre with only a handful of network providers starting to install DSF in metropolitan areas within Europe.

Theoretical analysis of chromatic dispersion limitations in lightwave transmission systems has been undertaken in the past [14] for both coherent and direct detection modulation schemes. For this application, we will consider only the analysis of direct detection schemes using on-off keying (OOK). The level of intersymbol interference is related to the amount of eye-diagram closure in dB. A chromatic dispersion factor is developed, corresponding to 1dB of eye closure and hence 1dB of dispersion penalty. The chromatic dispersion factor is given by :

$$\gamma = \frac{1}{\pi} \cdot B^2 \cdot L \cdot D \cdot \frac{\lambda^2}{c}$$

where B is the data rate, L is the fibre path length and c is the speed of light in a vacuum. It has been calculated that for a direct detection OOK modulated system, the chromatic dispersion factor, γ is 0.252 for 1dB eye closure penalty (or 0.321 for 2dB eye closure penalty). This information has been used to calculate the maximum transmission length for lightwave systems at bit rates from 1Gbps to 20Gbps as shown in Figure 4.15.

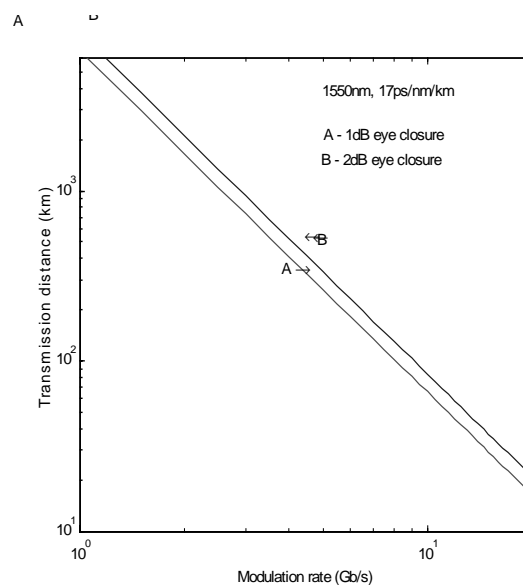


Figure 4.15 Maximum transmission distance for OOK digital signal for both 1dB and 2dB eye closure penalty

For signals at a rate of 1Gbps, the maximum transmission distance is approximately 5800km. This reduces to around 58km of dispersion limited distance for signals at 10Gbps.

4.2.7 Polarisation Mode Dispersion in Digital Optical Links

We have already seen that the dependence of refractive index on wavelength leads to chromatic dispersion in single mode optical fibres. Similarly, in real optical fibres, the

refractive index experienced by an optical signal will depend on the plane of polarisation of the light in the fibre. This is termed *birefringence* and leads to polarisation mode dispersion in fibres.

Figure 4.16 shows the basic mechanism for the generation of polarisation mode dispersion delay (PMD). At the transmitter end, the pulse is represented by the phasor sum of the x and y polarisation components. As these components propagate through the fibre, the inherent birefringence causes one of the components to be delayed with respect to the other. In high bit rate systems, this differential group delay can lead to signal distortions and hence a degradation in the BER of the received signal.

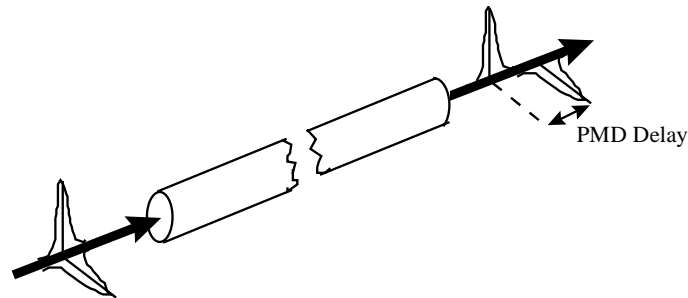


Figure 4.16 Group delay of two orthogonal polarisations after passing through a singlemode fibre

The group delay between two polarisation components is called the differential group delay. Its average is the PMD delay (in ps) and is expressed by the PMD coefficient in ps/ $\sqrt{\text{km}}$. The PMD does not increase linearly, but with the square root of transmission distance.

$$\Delta\tau = \sqrt{L} \cdot \Delta\tau_{\text{coeff}}$$

where L is the transmission distance and $\Delta\tau_{\text{coeff}}$ is the PMD coefficient. Taking into account the statistical character of PMD variations, if a 1dB power penalty due to PMD can be accepted then :

$$\Delta\tau_{\text{max}} \leq \frac{T}{10}$$

where T is the bit period. Setting T as $1/B$ we obtain :

$$L \leq \frac{1}{100 \cdot B^2 \cdot \Delta\tau_{\text{coeff}}^2}$$

where B is the bit rate. Figure 4.17 shows the outcome of the above equation. The transmission distance limitations increase with the square of the data rate and with the square of the PMD coefficient.

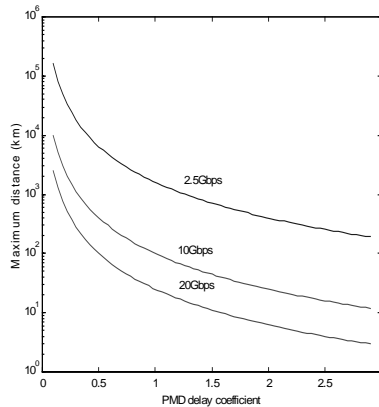


Figure 4.17 Maximum transmission distances for different data rates with varying PMD coefficients

From the calculations, it is clear that if we wish to transmit a 10Gbps signal over 100km, we require a fibre that can guarantee a PMD coefficient which is less than $1\text{ps}/\sqrt{\text{km}}$. This cannot be guaranteed with conventional single mode fibres so some form of PMD compensation must be applied.

Fibre manufacturers are reporting new fibres with vastly improved and guaranteed PMD coefficients. Recent examples include $0.5\text{ps}/\sqrt{\text{km}}$ and some manufacturers report that they can realise fibres with a delay coefficient of 0.1.

4.3 Development of MATLAB Graphical User Interfaces (GUIs)

For future ease of use, the system design algorithms have been implemented as GUIs within MATLAB. There are three front end GUI files, **rfgui.m** for analogue optical links, **diggui.m** for digital optical links and **diggui2.m** which performs the same calculations as **diggui.m** but shows graphical output of the accumulation of optical power (signal and ASE) at the output of cascaded EDFAs in the link. Each of these routines requires an additional MATLAB m-file which is called from the GUI and performs the calculations. These additional routines also pass back numerical and graphical information to the GUI.

A floppy disk is appended to the report of the files necessary to run these applications. These files listed below must be placed within the directory **C:/MATLAB/bin**

- rfgui.m** - Graphical user interface front end for analogue system analysis
- diggui.m** - Front end GUI for digital system analysis - no power monitor
- diggui2.m** - Front end GUI for digital systems including a trace of optical power
- digi1409a.m** - Algorithm file associated with **diggui2.m**
- digi1409.m** - Algorithm file associated with **diggui.m**

disper0712.m - Algorithm file associated with **rfgui.m**

Once these files are located in the named directory, the algorithms for analogue and digital design can be accessed via the GUIs as follows :

- Run the MATLAB application
- At the prompt, type in the name of the analysis GUI required e.g
>rfgui
- The screen which appears contains a number of input parameter boxes which are used to define the system parameters. When these have been entered, the CALCULATE button is pressed and the results are displayed either in a results field e.g for SNR, gain, IMD3 and noise figure etc or graphically (rfgui.m displays the frequency response of the link as would be displayed on a Vector Network Analyser as well as the RF power transfer characteristic curve)

5. ANALYSIS AND PERFORMANCE OF ANALOGUE OPTICAL LINKS

The following section will consider the feasibility of analogue optical systems for transmitting measurement data between telescope sites. Using the graphical user interface (GUI) written in MATLAB (filename **rfgui.m**) analysis was undertaken to examine the SNR distance limitation of an analogue optical implementation. Distances were increased in 10km stages from 20 to 500km. At each stage, the dynamic range was calculated. If the calculated dynamic range fell below the specified 14dB then a further EDFA stage was added and the calculation was continued. Figure 5.1 shows the result of the analysis

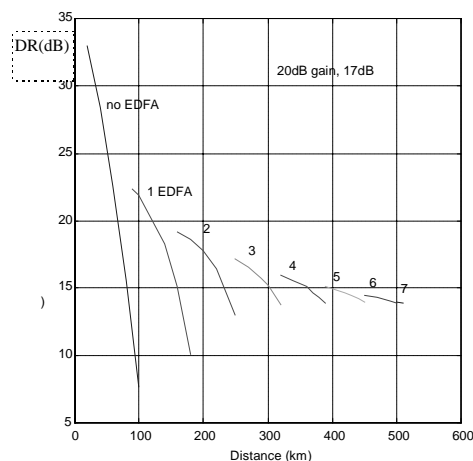


Figure 5.1 Analysis of long haul analogue links with multiple 20dB amplifiers

These results have assumed certain system parameters. The laser output power was chosen as high as possible to avoid non-linear effects and in particular SBS. A figure of 16dBm was calculated (and is available on the market). The RIN of the laser was set at -165dB/Hz (typical of a DFB laser) for operation at 1550nm. The modulator was assumed identical to the RAMAR device purchased by JBO which has an excess loss of 4.7dB, a quadrature loss of 3dB, V_{π} of 12v and a characteristic impedance of 26Ω . The detector had a responsivity of 0.875 A/W. The fibre was assumed to be standard single mode with a loss of 0.22dB/km and a dispersion of 17ps/nm.km. There was no

RF pre or post-amplification For dynamic range calculations, the maximum input RF power was defined to be 20dB below the input TOI and the minimum RF input power was selected to achieve a minimum SNR of 20dB. The EDFAs are all in-line amplifiers (filter bandwidth =1nm) placed equidistant to each other and from the transmitter and receiver.

It is clear from Figure 5.1 that there is a limit to the number of EDFAs that can be cascaded to achieve the required 14dB dynamic range. The EDFA gain was optimised at 20dB and the saturation output power was set at 17dBm (again available on the market). The distance limit of 505km could be improved upon slightly by increasing the saturated output power of the EDFAs but the limitation is mainly due to the build up of optical amplifier ASE, increasing the noise floor and thus reducing the SNR as EDFAs are introduced.

The above can be used as a design tool for analogue links over path lengths less than 500km. In terms of dispersion, the model predicts that for a 1GHz bandwidth signal at base-band the dispersion penalty is less than 1dB for distances in excess of 1000km. For a 2.5GHz bandwidth signal, this reduces to 200km whilst for a 10GHz signal the dispersion limit for a 1dB penalty is 15km. Assuming that the system operates over a 1GHz bandwidth, the link is attenuation limited (Figure 5.1) and there would be no requirement for dispersion compensation.

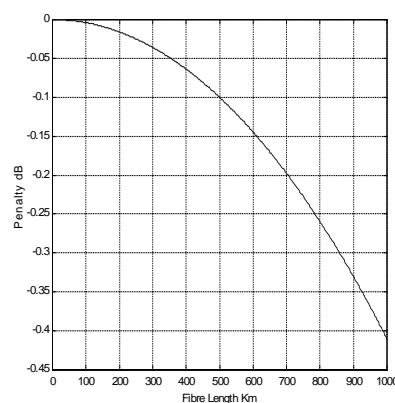


Figure 5.2 Dispersion penalty for 1GHz bandwidth signal over 1000km

The above analysis leads to the conclusion that if analogue links cannot be supported over path lengths greater than 500km then they are unlikely to be used within VLBI which requires transmission distances up to 3000km. It is true that the analogue option could be used to link telescopes within the distance limit such as Jodrell Bank to Cambridge within MERLIN, but it is likely that a standardised transmission protocol will be required throughout VLBI.

6. ANALYSIS AND PERFORMANCE OF DIGITAL OPTICAL LINKS

In a similar fashion to Section 5, the following will investigate the performance of digital optical links and their feasibility for Connecting European VLBI telescopes in real time. The following analysis was completed using the MATLAB graphical user interface developed (filename : **digigui2.m**). For each distance, the SNR was calculated. If at any point the SNR dropped below 20dB (SNR required for 10^5 BER), then a further amplification stage was added and the calculations were continued.

Figure 6.1 shows the results of the analysis up to a distance of 900km. The calculations were performed using a laser power of 10dBm, a modulator excess loss of 4.7dB and quadrature loss of 3dB. The fibre was assumed to have a loss of 0.22dB/km with a dispersion of 17ps/nm.km. All EDFAs were positioned equidistant from each other in the link. In addition, the transmitter and receiver were positioned at identical distances from the first and last EDFA . Each of the optical amplifiers had a gain of 20dB and a saturated output power of 17dBm with an optical filter bandwidth of 1nm to reduce the accumulation of ASE. The detector was assumed to have a responsivity of 0.875 A/W and the data rate was assumed to be 1Gbps.

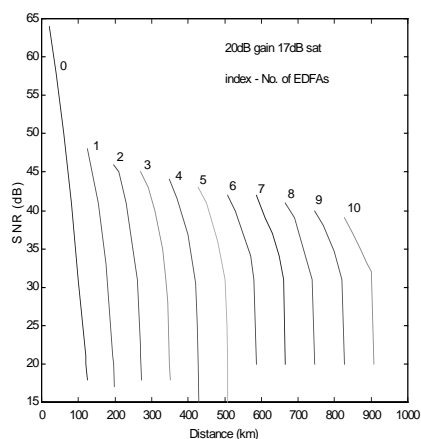


Figure 6.1 Analysis of SNR performance for cascaded EDFAs with gain=20dB, P_{sat} =17dB and a 1nm filter bandwidth. Data rate =1Gbps

When compared to the analogue analysis it is clear that the digital optical implementation allows the specification to be met over a much greater distance. In this study we are interested in the application of such links over distances as great as 3000km and so the above analysis can be extended to much greater fibre lengths as shown in Figure 6.2.

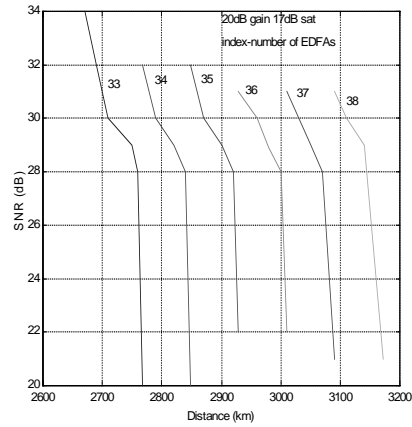


Figure 6.2 Continuation of above analysis for distances around 3000km.

It is clear from Figure 6.2 that the entire span of 3000km can be accommodated assuming a data rate of 1Gbps and identical component characteristics to that described above. The above system architecture takes advantage of the flexibility of EDFA technology. If at any time in the future, there is a requirement for more wavelength channels (WDM) or higher bandwidth, the system will allow such an upgrade with minimal capital investment. If however, there is no perceived requirement for multiple wavelength channels then a cascade of regenerators would be an option. This will be discussed fully in Section 8

7. EXPERIMENTAL MEASUREMENTS AND VERIFICATION

7.1 Introduction

The following section reports measurements taken experimentally within the scope of the work. These measurements fall into three categories: verification of the modulator characteristics, measurement of gain, SNR and noise characteristics of systems and phase stability measurements.

Verification of the modulator transfer characteristic is important to ensure that the correct operating point (quadrature point) is selected during system experimentation. Use of an incorrect operating point can lead to large mismatches between measured and predicted SNR and can also lead to non-linearities in the output signal. The second of the above categories involves the measurement of gain, noise characteristics and SNR. For both the analogue and digital models, the SNR is the most important characteristic for understanding the performance of the links. If the gain, noise and SNR measurements can be predicted accurately by the model, then there is increased confidence that the model can correctly simulate the performance of real optical systems.

Phase stability is an important factor for analogue optical systems used for radio astronomy. Phase instabilities between data streams at the correlator can cause de-correlation and degradation of the measured data. A de-correlation of around 1% is acceptable for radio astronomy measurements, which represents a phase error of around 7° . The work undertaken within this programme represents a preliminary investigation and includes the design of an automatic measurement set-up using GPIB and LABVIEW.

7.2 Measurement of V_π of Optical Modulator

Figure 7.1 shows the experimental set-up to verify the V_π of the optical modulator. The laser is a highly stable SANTEC tuneable source operating at 1550nm and an output power of 0dBm. This is connected by single mode polarisation maintaining fibre to the input PM pigtail of the RAMAR modulator. Bias to the modulator is supplied by a variable DC power source. Optical power is monitored using the power meter setting of the HP E6000A mini-OTDR.

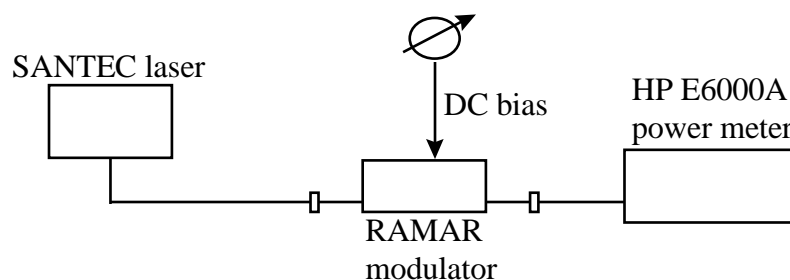


Figure 7.1 Experimental set-up for verification of modulator characteristics.

Figure 7.2 is a plot of optical power against bias voltage showing the co-sinusoidal nature of the transfer characteristic.

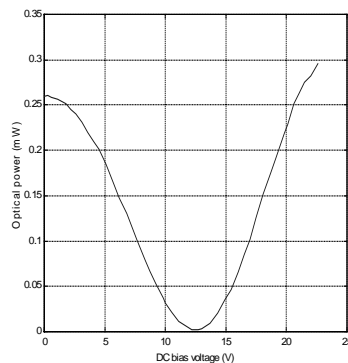


Figure 7.2 Experimental transfer characteristic for RAMAR modulator

From the figure, V_{π} can be defined as the voltage difference between the maximum and minimum transmitted optical powers. In this case V_{π} is 12 volts, which leads to a quadrature point voltage of 6 volts. This figure is used to set up subsequent experiments and also to define the modulator characteristics within the model.

7.3 Comparison Between System Experiments and Simulation

Figure 7.3 shows the experimental arrangement used to verify the modelled gain, noise floor and SNR. The laser is the same as used in section 7.2 with its optical power varied between -10dBm and 7dBm. The modulator was set at its quadrature bias point as defined in the previous section. The photodetector was an HP lightwave convertor with a responsivity of 0.875 A/W, operated at a bias voltage of 14V. A bias tee was connected to the electrical output of the detector and a 50Ω load was used to provide a dc path. The spectrum analyser was connected via a nominal 40dB gain amplifier with a bandwidth of 800MHz and a measured noise figure of 6.34 dB. An RF source provided a variable power microwave signal with centre frequency 490MHz.

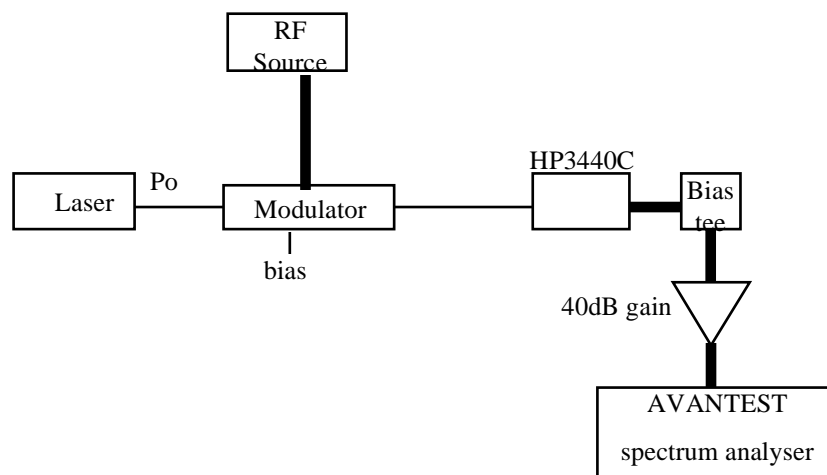


Figure 7.3 Experimental arrangement for measurement of system parameters

The spectrum analyser was set up at a centre frequency of 490MHz with a resolution bandwidth of 1MHz and a video bandwidth of 1KHz. The span was 100MHz and the sweep parameter was 200ms. No additional fibre loss was connected after the modulator in these tests unless mentioned. Table 7.1 compared the measured system gain against that calculated using **rfgui.m** for identical system parameters, over a range of optical powers. There is excellent agreement between the figures as shown by the graph of Figure 7.4

Table 7.1

Optical Power (dBm)	Measured gain (dB)	Calculated gain (dB)
-10	-42.5	-42.6
-7	-37	-36.6
-3	-29.3	-28.6
0	-23.1	-22.6
3	-16.5	-16.6
6	-10.5	-10.6
7	-8.4	-8.6

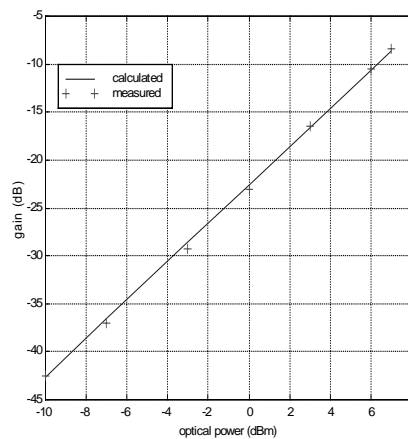


Figure 7.4 Comparison of measured and calculated gain

Next the system noise floor was measured and calculated assuming a bandwidth of 1MHz and including contributions from thermal noise, shot noise and RIN. Table 7.2 shows the comparison between measured and calculated results.

Table 7.2

Optical power (dBm)	Measured noise (dBm)	Calculated noise (dBm)
-10	-71.8	-71.5
-6	-71.5	-71.3
-2	-70.62	-70.85
0	-70.6	-70.65
2	-70.4	-70.4
4	-70.2	-69.9
6	-69.9	-69.3

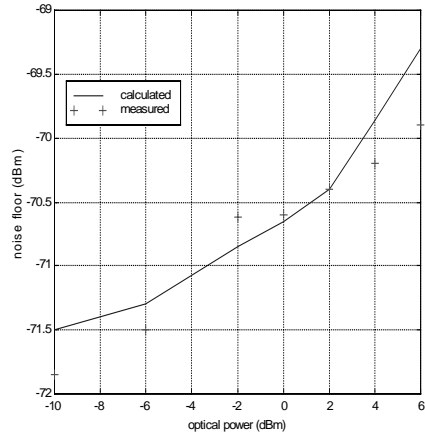


Figure 7.5 Comparison of calculated and measured noise floor values

The error standard deviation between measured and calculated results is of the order of 0.26dB.

Perhaps the most important comparison is that between the measured and calculated SNR. Table 7.3 tabulates these results whilst Figure 7.6 plots them graphically.

Table 7.3

Optical power (dBm)	Measured SNR (dB)	Calculated SNR (dB)
-10	13	13.8
-7	18.5	19.7
-3	26.2	27
0	32.4	33
3	39	39
6	45	44.1
7	47	46

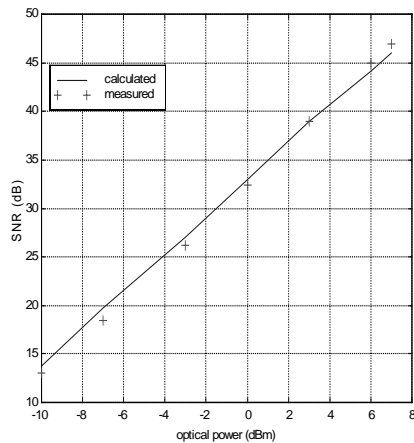


Figure 7.6 Comparison between measured and calculated SNR

There is excellent agreement between the measured and calculated results suggesting that the models will be able to predict the performance of real optical systems with acceptable accuracy.

At the time of writing, verification of system models with optical amplifiers was not possible due to the fact that the required EDFA had not been delivered to Jodrell Bank by the promised date.

7.4 Experimental Verification of Dispersion Characteristics

The simulation routine **rfgui.m** includes a set of algorithms for predicting the trace that would be produced on a Vector Network Analyser. This is useful for long haul analysis to understand the effect of chromatic dispersion and also to take account of the frequency roll off of the optical components in the link. The following section describes the results of measurements undertaken to verify that the model is representative.

Figure 7.7 shows the set-up for the measurements. The laser, modulator and detector were as previously described. Initial measurements were performed with the 30km fibre reel disconnected and a straight through connection from the modulator pigtail fibre to the photoreceiver. Figure 7.8 shows the measured trace which represents the frequency roll off of the optical components over the range 0-20GHz.

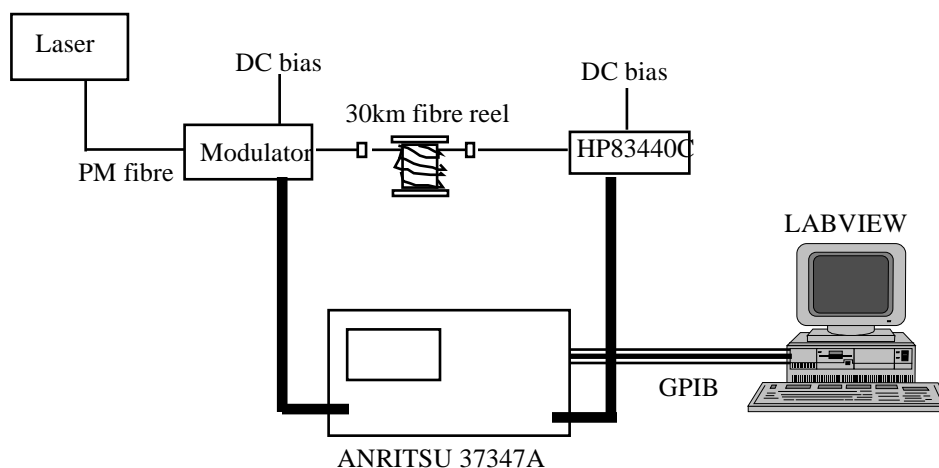


Figure 7.7 Experimental arrangement for frequency and dispersion analysis

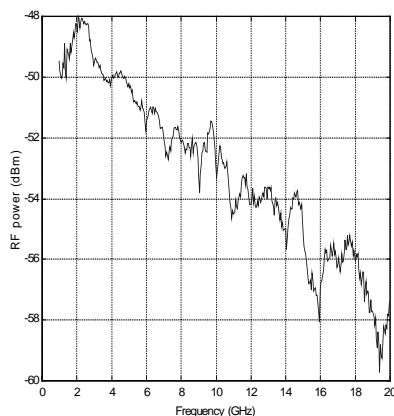


Figure 7.8 Frequency response of the modulator and photoreceiver

The data from Figure 7.8 allowed the model to be updated to take account of optical component frequency roll off.

With this addition to the model in place a comparison was made between the trace predicted by the model for a link with 30km of fibre and the measured response. The length of the fibre was measured with good accuracy using an OTDR and the loss was measured using the same instrument in optical power meter mode. The actual dispersion of the fibre used was not directly measured but was estimated to be in the region of 17ps/nm.km.

Figure 7.9 shows the result of the comparison for the 30km link. The predicted response is fairly accurate keeping in mind that the modelled dispersion parameter was estimated rather than measured.

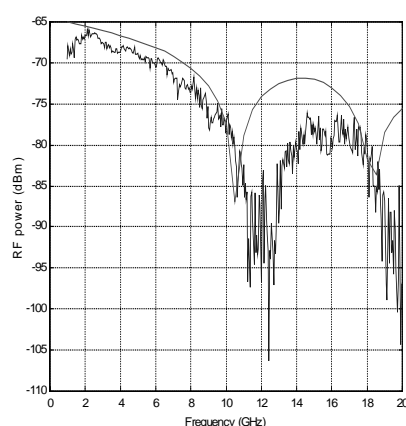


Figure 7.9 Comparison of measured and calculated frequency response for a 30km link including contribution from optical components.

7.5 Experimental Phase Stability Measurements

Phase stability is of major importance to ensure coherent processing of radio astronomy data at the correlator. Experiments have been undertaken within the scope of this study to measure the effect on an analogue optical link. It is generally accepted that two data paths should not be out of phase by more than 6° to avoid decorrelation of the output by more than 1%. Experiments were undertaken using the arrangement shown in Figure 7.10. A vector network analyser was used to take advantage of its highly stable RF source over the frequency range 0.4 - 20GHz. There was the added advantage that the internal RF source of the analyser could be frequency locked to a local Maser source if required to reduce the inherent phase noise from the instrument.

Since the network analyser in question is not able to provide a direct measurement of phase over time (where 'phase' refers to the difference in phase between the internal reference of the instrument [port1 to port 2] and the measurement path from modulator to photoreceiver), the GPIB facility was used along with LABVIEW (**tester.vi** on disk) to extract the relevant data from the analyser and save this to a data file for subsequent plotting. Figures 7.11 to 7.14 show the effect of increasing fibre path length (up to 30km in the lab) on the relative phase stability of the analogue

signal. It is clear that above a certain fibre path length, the phase stability would not be within the required radio astronomy limitations for an analogue link.

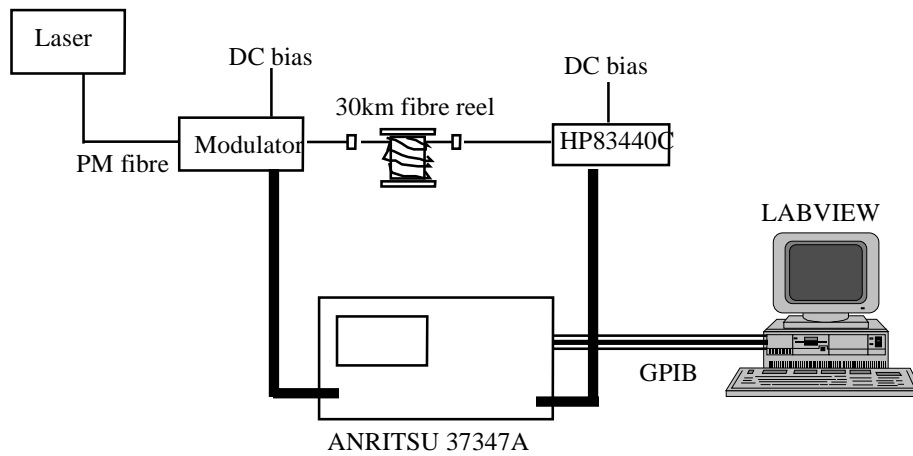


Figure 7.10 Experimental set up for phase stability measurements

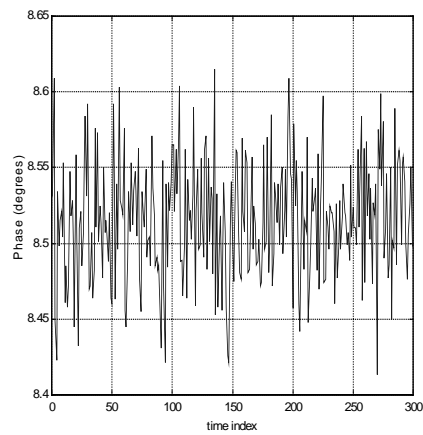


Figure 7.11 Phase jitter characteristics with 0km of fibre (over ~3minutes)

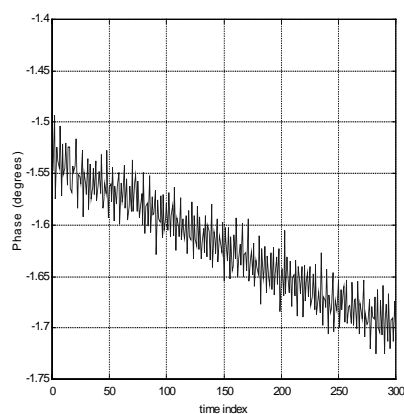


Figure 7.12 Phase jitter for 6.4km fibre reel (~3minutes)

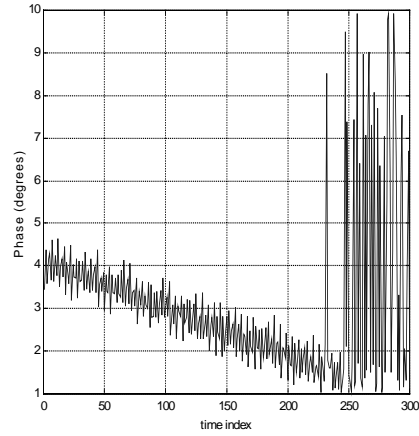


Figure 7.13 Phase jitter over 12km fibre reel (3minutes)

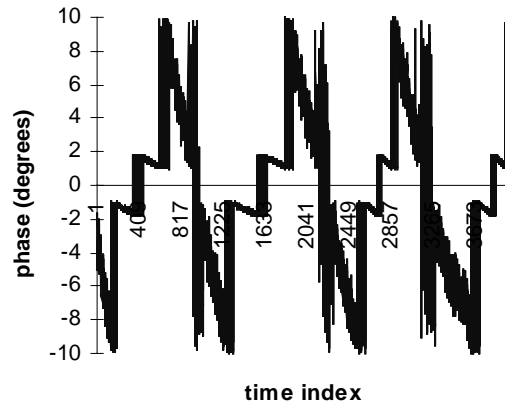


Figure 7.14 Phase jitter over 30km fibre reel (30minutes)

8. EXAMPLE LINK : PERFORMANCE AND COST ISSUES

As an example, consider a link between Effelsberg and Dwingeloo which has a tracked dark fibre path length of approximately 300km. We have concluded already in Section 5 that analogue techniques cannot deliver the performance required by the European VLBI Network and so it is not worthwhile analysing a single link for the analogue case, if the whole network cannot be interconnected in this way. Furthermore, data from the Effelsberg telescope will already have been digitised on site prior to VLBI recording. For these reasons, we will consider only a digital transmission scheme.

There are two equipment options : (i) Implementation of the link using standard SDH equipment and electronic re-generators and (ii) Implement using EDFAs. The first option is the simplest but would make upgrading to a full system implementation at a later date a difficult task. This is because the full EVN will require a WDM system and re-generators would be required for each wavelength (costly). The second option using EDFAs in the link is likely to be more expensive but will make a full system upgrade easier / less expensive.

Assuming a data rate of 1Gbps over the link, a regenerated SDH system would require 4 repeaters if the incident laser power is 0dBm. If a higher laser power is available (say 10dBm) then the distance can be covered by 3 repeaters to achieve the required 20dB signal to noise ratio (and equivalent BER). However since most commercially available SDH systems work at 2.5Gbps, some form of bit rate conversion would be required at each end. This would not affect the number of repeaters in the link but will slightly degrade the received BER.

Using a custom EDFA system would allow transmission at a bit rate of 1Gbps and over the path length in question, would require 3 optical amplifiers (see Figure 6.1) assuming a laser power of 10dBm. This configuration with 20dB gain EDFAs (which saturate at 17dBm), can deliver a signal to noise ratio exceeding 40dB.

For the above two examples, we can estimate the costs of implementing the link. In both cases fibre spurs will have to be built at both sites to reach the nearest telecommunication point-of-presence (POP) The cost of this has been estimated by extrapolating the budgetary costs supplied for the same activity in the UK but over a slightly longer distance. The dark fibre lease cost is a one-off and is calculated on the basis of similar (per km) costs for the UK. Equipment costs do not refer to component costs but to an estimate of the cost of a commercially available sub-systems (SDH and EDFA). A small additional cost has been added for maintenance.

SDH Regenerators (£ K)	EDFAs (£ K)
------------------------	-------------

fibre spurs	330	fibre spurs	330
fibre lease	1800	fibre lease	1800
equipment	120	equipment	170
other	50	other	50
Total	2300	Total	2350

Table 8.1 Relative costs for single link systems using SDH regenerators or EDFAs

It is clear that there is little difference in cost between the two options and that if a one-off demonstration link between Effelsberg and Dwingeloo was to be considered, then a budget in excess of £2.4 million would be required.

9. IMPLEMENTATION ISSUES

9.1 Pre-installed Leased Dark Fibre

One option for implementation is to lease pre-installed dark fibre from a fibre provider. As an example, Figure 9.1 shows the optimum fibre route from Jodrell Bank to Cambridge using pre-installed fibre. The red sections of the diagram show where fibres will require to be laid to connect the telescope to the nearest Point-of –Presence (POP).

The advantage of this route is that minimum build work is required because the fibre has been installed by the provider. The disadvantages include the fact that the span length is not minimised and for this case is approximately 400km compared to the 217km direct crow-flies distance. This will have an effect of the number of repeaters / EDFAs used in the link.



Figure 9.1. Example of pre-installed dark fibre routing between Jodrell Bank and Cambridge.

9.2 Self-build Option

Another option, which may be of benefit in the longer term is to consider building the fibre network. In this way the fibre will be owned by the radio astronomy community (PPARC / JIVE). An additional benefit of this implementation route is that the fibre span length can be optimised and hence the number of repeaters / EDFAs can be kept to a minimum. The major advantage in this case is that the fibre is wholly owned and so bandwidth can be re-sold into the communications market to provide a return on the original investment made during installation. With the current boom in high bandwidth communications for internet applications, it is feasible to assume that the

income generated from such a venture could sustain the upkeep of the link and financing of future upgrades. Figure 9.2 shows an example of how Jodrell Bank could be connected to Cambridge. The fibre laying costs would be minimised using a patented technique (Micro-Cabling) which installs the fibre in a six-inch groove cut into the side of major carriageways. Access to way-rights would not be required if public highways are used and 'code-powers' have been obtained (i.e a telecommunications licence). At the time of writing the micro-cabling technique has not been approved in the UK but has been used in France and Germany.

There are several MAJOR disadvantages of this method :

- JIVE would require a telecommunication licence in 10 countries within Europe
- Micro-cabling could be laid at a maximum rate of 1km / day. Within EVN there is a requirement for over 7000km of fibre network which would mean that at full speed, the process would take approximately **20 years !!!!**



Figure 9.2.Self build option showing fibres laid along major roadways.

9.3 Available Optical Fibre Capacity Within Europe

The above examples consider the implementation issues for interconnection of telescopes within the UK. This is a valid consideration when discussing the feasibility of interconnecting EVN telescopes since the current Jodrell to Cambridge connection represents the weak link in European VLBI by virtue of its limited microwave bandwidth. Connecting these two sites could be regarded as the first step in an EVN upgrade.

It is important to consider how the entire European VLBI network might be connected in the near future (see section 9.4). To assist in this activity, Corning have kindly tracked dark fibre availability in Europe based on known points of presence and grid

references of the VLBI stations. Figure 9.3 shows a map of communication hubs throughout Europe and information has been supplied detailing the self build ‘spur’ distances that would be required to connect each of the sites to the nearest point of presence (Table 9.1).

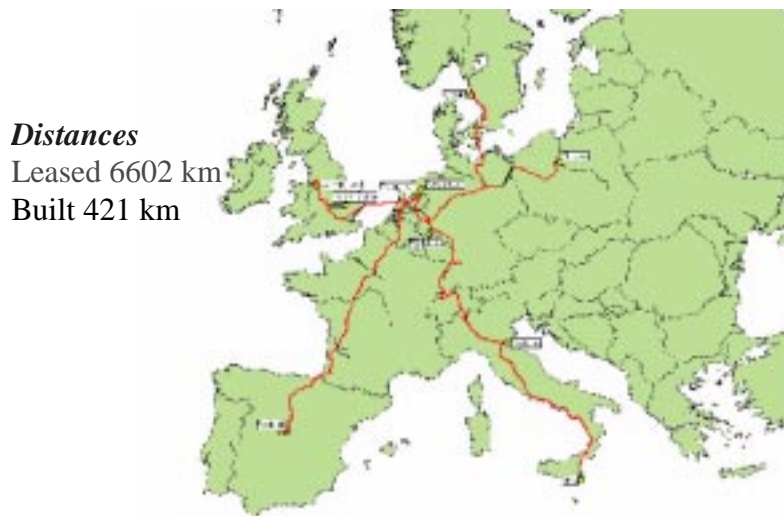


Figure 9.3. Available dark fibre capacity within Europe for EVN

It is likely that the lowest cost route to full European interconnection will make use of pre-installed dark-fibre. It is unlikely that future project budgets will extend to a Euro-wide self-build option (see section 9.2). The implementation used will be dependent on the requirement for data transfer (synchronous or asynchronous). Since the current technique is essentially asynchronous, then some form of packet switched fibre ring network would be compatible. There are future plans for a European wide fibre ring network servicing academic research institutions.

Telescope Locations	Fibre Provider(s)	Straight line build distance to POP
Lords Bridge (Cambridge)	Fibreway Racal	6.2 km - Cambridge
Westerbork, Netherlands	Versatel	32.8km -Groningen
Onsala, Sweden	Hermes Euro Rail	35.5km - Goteborg
Medicina, Italy	Societa Autostrade Albacom Adriacom Telecom Italia WIND	116km - Venice
Robledo, Spain	RENFE	66km - Chinchilla de Monte Aragon (194kms to Valencia or Madrid)
Effelsberg, Germany	Viatel Versatel GasLINE	25.8km - Bonn 46km - Koln 46km - Level 3
Pinwice, Poland	Polish State Railways	39km - Bydgoszcz
Dwingeloo, Netherlands	Versatel Versatel	39.4km - Zwolle 46.5km - Groningen
Noto, Italy	Societa Autostrade Telecom Italia	68km - Catania

Table 9.1 Distances from telescopes to nearest telecoms 'hub' and relevant fibre providers. (Multiple pan European carriers are available to bring traffic across the long haul sections)

9.4 Full Network Costs

There are three options that should be considered for connecting up the entire VLBI network. :

Standard SDH Technology at 2.5Gbps

- Currently available commercial SDH technology could be used, which will require the lease of multiple dark fibres and the provision of in-line regenerators along the route. The data rate for this solution will be limited to 2.5Gbps per channel based on available technology. Figure 9.4 shows a schematic of the required system

The number of SDH repeaters in figure 9.4 has been calculated under the assumption that the data rate is 2.5Gbps. Under these circumstances, and assuming a laser power of 0dBm at each of the transmitters, a regenerator is required at approximately 80km intervals in the link. Table 9.2 shows the estimated costs of implementation (based on March 2000 figures supplied by Corning in relation to e-MERLIN upgrade)

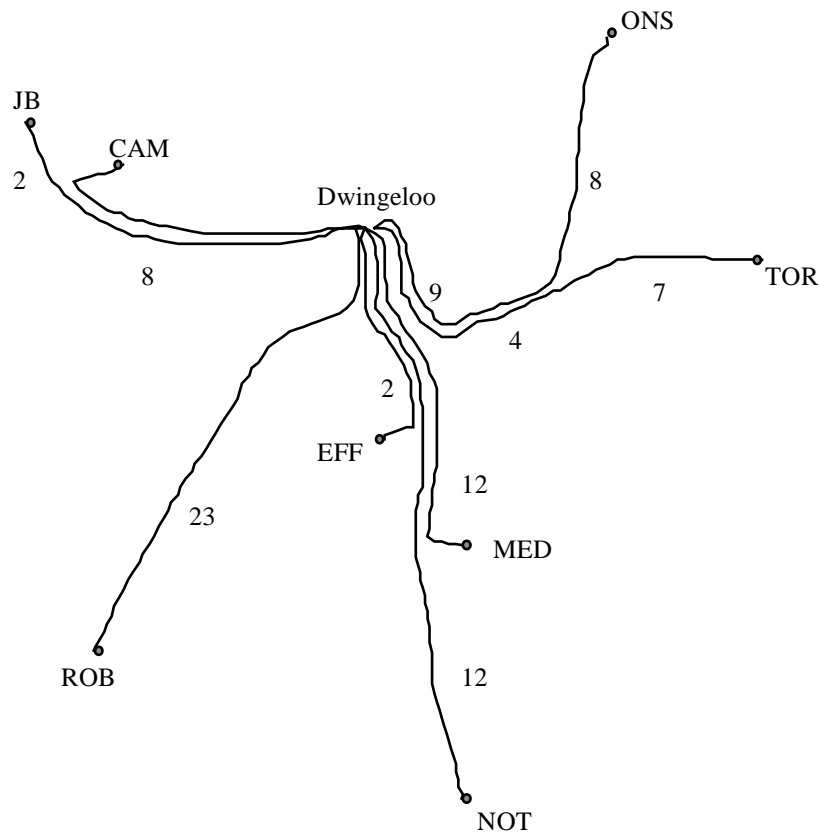


Figure 9.4 Network configuration for standard SDH technology with repeaters.
Number of repeaters shown in each path

Item	Cost (£ Million)
------	------------------

fibre spurs	2
fibre lease	60
equipment	3
Total	£65 Million

Table 9.2 Estimated costs for EVN interconnection using standard SDH technology

Single Fibre DWDM using EDFAs up to 10Gbps

- This option will also require the construction of identical fibre spurs to points of presence in the network. The calculations are based upon using Wavelength Division Multiplexing (WDM) over leased dark fibre. In such a system, each telescope site requires a unique highly stable laser source. The data from each site is multiplexed onto the fibre at add-drop-multiplexers (ADMs) within the network. The equipment costs are based on estimates for fully monitored and controlled commercial optical amplifier sub-systems

Figure 9.5 shows a network schematic for the optically amplified case. The blocks located at the nodes of the network correspond to add drop multiplexers (ADMs). A wavelength selective filter unit is also required at the receiver in Dwingeloo to separate out the signals from each of the telescopes. The number of optical amplifiers is based on a laser power of 10dBm and one amplifier per 100km of fibre.

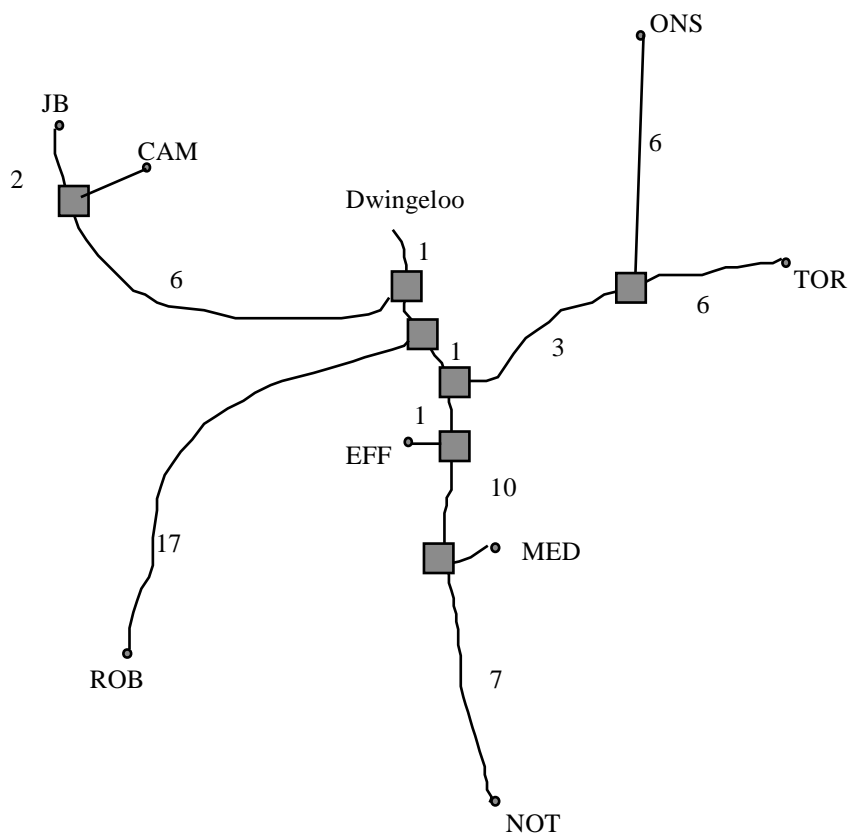


Figure 9.5 Network architecture for optically amplified DWDM system. Numbers of optical amplifier units are noted in the link.

Item	Cost (£ Million)
------	------------------

fibre spurs	2
fibre lease	60
equipment	3.5
Total	£65.5 Million

Table 9.3 Estimated costs for EVN interconnection using optical amplifier technology and DWDM

Use of European Research Institution Ring Network (Planned under IST programme) up to 10Gbps

- There is a possibility that the European Commission will fund the construction of a vast high capacity ring network servicing the data transmission requirements of the major research institutions within continental Europe. This may include sites such as CERN, RAL, Daresbury etc. The ring network is likely to have open system connections into the commercial network and so EVN may be able to access the high capacity fibre ring via commercial traffic routes. The EVN data would be transmitted asynchronously through the network with relevant timing headers and routing information to be re-constructed and stored/processed at the correlator. In this way either correlator (Dwingeloo or Bonn) could be used by simply re-routing the data. Fibre spurs would still require construction to nearest points of network presence and the links would incur running costs per year for traffic sent through the system. Figure 9.6 shows a possible schematic arrangement

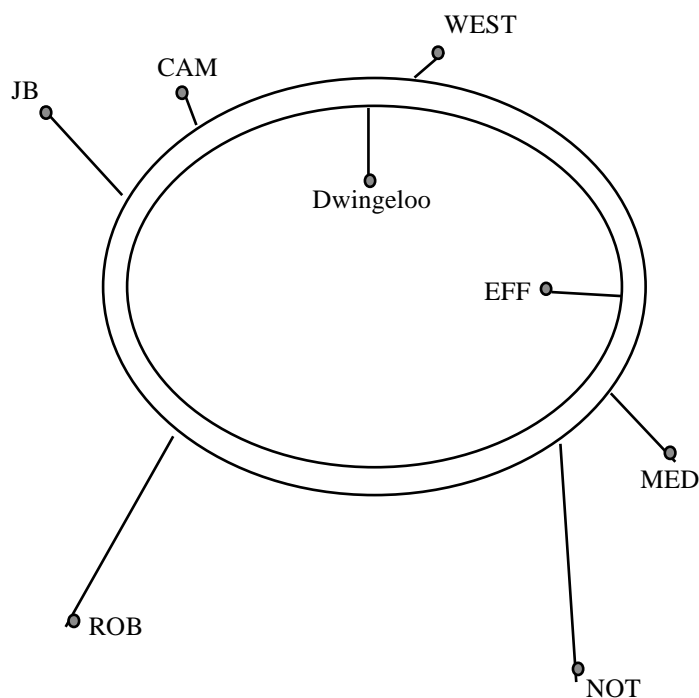


Figure 9.6 EVN connected through European high capacity ring network constructed under IST funding

Item	Cost (£ Million)
fibre spurs	2
equipment	1
Total	£3 Million

Table 9.4 Estimated costs associated with using European ring network

It is essential that if JIVE wishes to pursue this route, that the consortium is involved in the system definition stage of any IST programme. It is not known what the planned timescale for such a development would be. The above costs may be significantly lower than the actual if dark fibre is required to be leased to reach the ring network (this may be the case with the Noto and Robledo sites).

10. CONCLUSIONS

The increase in availability of installed optical fibre within Europe is presenting a unique opportunity to upgrade the European VLBI Network. There are clear advantages to replacing the current recorder technology with an optical fibre network. These include earlier availability of scientific results and perhaps more importantly, increased efficiency during the measurement sessions.

This report has investigated the feasibility of interconnecting the EVN with optical fibres. The work involved the construction of optical device and system models in MATLAB script for both analogue and digitally modulated optical links. These models were used to predict the performance of optical links over distances in excess of 3000km, taking account of chromatic dispersion, non-linear phenomena such as SBS and polarisation mode dispersion if appropriate. In addition to the theoretical modelling, experimental work has been performed to verify correct operation of the models and better characterise phase instabilities for the analogue case. Furthermore, contact has been made with the optical fibre industry to investigate the availability of dark fibre across the EVN span and close to the VLBI station sites leading to cost estimates for both a single experimental link and full network implementation.

The major conclusions drawn from the work are as follows :

- The models predict that analogue modulation will only perform adequately over distances not exceeding 500km (assuming a 1GHz bandwidth). For signals with greater than 1GHz bandwidth, it is not possible to achieve the specified performance over more than ~150km. For this reason, it is concluded that analogue modulation is not suitable for optical links interconnecting the EVN.
- Modelling has shown that for a digital system operating at 1Gbps, optical amplifiers can be cascaded over distances in excess of 3000km without significant degradation in system performance and without dispersion compensation. Higher bit rates can easily be accommodated with careful attention to the effects of polarisation mode dispersion and chromatic dispersion in the links. Digital modulation is therefore deemed to be suitable for the application.
- Although models have predicted that analogue links are perfectly feasible for short haul optical links, experimental work has shown that transmission of wide band data signals using analogue modulation is complicated by the phase instability of the signal, which degrades with fibre length. This would lead to de-correlation of data. Furthermore it would be difficult to phase correct for a wide band signal using a feedback control system.
- Dark fibre is available throughout continental Europe and has been tracked to network points close to the VLBI sites. Full network connection requires the lease of 6602km of dark fibre. Connection of each of the sites considered to a network point would require installation of around 440km of optical fibre. A low cost installation technique is available within Europe (not yet approved in UK). 'Micro Cabling' uses a 7 in deep groove in roadways which is loaded with the fibre and back filled. A telecommunications licence would be required in each country where Micro-Cabling was to be used.

- There are three potential network implementation schemes :
 - Multi-fibres with standard commercial SDH equipment : This requires a separate fibre for each telescope site. Each fibre requires SDH transmit / receive and repeater sites. At the moment this equipment is restricted to 2.5Gbps.
 - Multi-wavelength (DWDM) communications link on single fibre backbone : This has the advantage of flexibility and is capable of future upgrades. Equipment is becoming available for multi wavelength systems operating at 10Gbps per wavelength. Expect future upgrade to 40Gbps per wavelength.
 - There are plans for the construction of a large fibre ring network throughout the major research institutions within continental Europe. This may be part funded by the European IST programme. Assuming that this ring network is constructed, telescope sites could be connected (requires construction of fibre spurs to network points), providing an asynchronous, packet switched communication link between sites and any correlator. There is no current information on the planned network speed / capacity.
- Implementation of the first two fully connected network schemes requiring the lease of dark fibre is likely to cost in the region of £65 Million.
- Implementation of a link which 'piggy-backs' on the IST European ring network could cost as little as £3 to 5 Million.

11. REFERENCES

- [1] R. Spencer et al, "The use of optical fibres in radio astronomy", Accepted by Journal of Modern Optics, November 1999.
- [2] J. Amagai et al, "Preliminary experiments of radio interferometer using fibre optic links modulated in radio frequency", Communications Research Laboratory, Technical Development Center News, No. 10 pp 22-24, May 1997.
- [3] H. Kiuchi et al, "Real time VLBI via the STM-16 ATM network", Communications Research Laboratory, Technical Development Center News, No.15, pp 12-15, Nov. 1999.
- [4] N.A. Olsson, "Lightwave systems with optical amplifiers", J. Light Tech, Vol.7, No. 7, pp 1071-1081, July 1989.
- [5] C.R Giles, "Propagation of signal and noise in concatenated erbium doped fibre amplifiers", J. Light Tech., Vol. 9, No. 2, pp 147-154, Feb. 1991.
- [6] A. Yariv, "Signal to noise considerations in fibre links with periodic or distributed optical amplification", Opt. Lett. Vol. 15 No. 19, pp 1064-1066, Oct. 1990.
- [7] W.E Stephens et al "System characteristics of directly modulated and externally modulated RF fiber optic links", J Light Tech. Vol. 5 No. 3, pp 380, March 1987.
- [8] U Gliese et al, "Chromatic dispersion in fibre optic microwave and mm-wave links", IEEE Trans Microwave Theory, Tech Vol. 44 No. 10, pp 1716-1723, Oct. 1996.
- [9] G.H Smith et al "Overcoming chromatic dispersion effects in fibre wireless systems incorporating external modulators", IEE Trans Microwave Theory Tech. Vol. 45 No.8, pp 1410-1415, Aug. 1997.
- [10] H. Schmuck, "Comparison of optical mm-wave system concepts with regard to chromatic dispersion", Elect. Lett. Vol. 31 No. 21, pp 1848-1849, Oct. 1995.
- [11] R.H Stolen, "Nonlinearity in fibre transmission", Proc. IEEE Vol. 68 No.10, pp 1232-1235, Oct. 1980.
- [12] X.P Mao et al, "Brillouin scattering in externally modulated lightwave AM-VSB CATV transmission systems" IEEE Phot Tech Lett. Vol. 4 No.3, pp 287-289, March 1992.
- [13] A.R. Chraplyvy, "Limitations on lightwave communications imposed by optical fibre nonlinearities" J. Light Tech. Vol. 8 No.10, pp 1548-1557, Oct. 1990.
- [14] A.F. Elrefaie et al, "Chromatic dispersion limitations in coherent lightwave transmission systems", J. Light Tech. Vol. 6 No. 5, pp 704-709, May 1988

APPENDIX A. PHASE PERFORMANCE OF FIBRE LINKS

1) Introduction.

Measurements of the phase stability of a fibre link in the laboratory was described in section 7.5 of the main report, where it was concluded that the phase performance of an analogue link was poor. This result in fact contradicted the conclusions reached by Dr Lucia Hu based on measurements on both laboratory and installed fibre links in our joint PIPSS project with BT Laboratories.

However subsequent tests with the equipment described in section 7.5 showed that the network analyser was unstable, having a periodic frequency shift of 2 kHz at a carrier frequency of 10 GHz, even when locked to the external H maser frequency standard. This modulation occurred at around 0.5 Hz and interfered with the phase measurements. The rms phase measurements in these experiments were therefore overestimates. New measurements were required in order to find the actual performance.

2) The New Measurements.

We therefore decided to repeat the measurements using an HP vector voltmeter (VVM) to measure the phase, with a frequency synthesiser locked to the maser and operating at 1 GHz (see figure 1). A PC with a GP-IB interface collected the data at 0.96 second intervals (set by internal timing in the program). This will be taken as the unit of time in the discussion which follows and treated as a nominal second.

Data were taken in a number of runs over the period 16 June – 11 July 2000. Each run took 5000 data points (4800 seconds). Programs were written in MathCad to calculate Allen variance (see e.g. Thompson, Moran and Swenson 1986) and power spectra. An additional program (in C) produced results more directly relevant to VLBI: 1) the variation of rms phase deviation from a straight line fitted to n data points vs n , 2) a coherence function vs n . Case (1) corresponds to the situation in VLBI when fringe rate and delay are fitted to the interferometer output for each scan on a source. The coherence function in case (2) is obtained by a vector sum of data points with unit amplitude and assigning a phase equal to 100 times the measured phase, i.e. equivalent to a coherence measurement at 100 GHz.

3) Results and Discussion.

Figure 2 shows the typical phase behaviour over one of the runs with a 30 km link at 1 GHz. The rms phase deviation over this run was 17.3 degrees about a mean of -47.3 degrees. Figure 3 shows the Allen standard deviation. This falls off as $(\text{lag})^{-1}$, corresponding to a random walk in phase, reaching a plateau at ~ 30 seconds. The plateau is consistent with thermal drift due to small temperature changes in the laboratory and a thermal coefficient of 10^{-5} . The power spectrum (figure 4) falls off as $(\text{frequency})^{-2}$, reflecting a random walk in length corresponding to the thermal drift. Similar features were seen in all data except for the 0 length fibre case (see below).

The fibre supplied was in drums of 6.4 and 8.8 km. Data were collected for increasing lengths of fibre (each drum connected by means of FPC connector pig-tails fusion spliced onto the fibre on the drum), and the results summarised in Table 1. Column 1 indicates the length of fibre, columns 2 to 5 give the results of the C program, where columns 2, 3 and 4 give the values for the mean rms phase deviation from 5, 50 and 500 data points respectively, and column 5 the integration time $T(c=0.5)$ in seconds for which the coherence function drops to 0.5 (assuming a frequency of 100 GHz as stated above). Column 6 and 7 show the results of the Mathcad program, giving the value of the Allen standard deviation (ASD) for a lag of 10 seconds, and the approximate lag in seconds where the plateau is reached.

Table 1 Results of Lab measurements on varying fibre lengths.

Length m	rms degrees	5 rms degrees	10 rms degrees	500 rms degrees	$T(c=0.5)$ sec	ASD	lag(plateau) sec
2	0.021	0.037	0.045	>3200		2×10^{-14}	----
6400	0.037	0.061	2.2	250		3×10^{-14}	30
15200	0.051	0.074	3.9	90		3.5×10^{-14}	35
21600	0.068	0.097	2.6	190		5×10^{-14}	40
30200	0.099	0.14	6.89	60		7×10^{-14}	25

The trend of rms phase deviation with increasing time scale and fibre length can be seen. The coherence time for the measurement system alone i.e. output of the modulator connected to the detector by 2m of fibre was longer than the record length analysed. The rms phase deviation over the whole run was 0.093 degrees at 1 GHz. No plateau was present in the Allen variance, showing that thermal drift was not important for the measurement system. The power spectrum had a flat section at low frequency, and did not show the power law behaviour seen for the fibre on the drums and shown in figure 4.

The coherence time increases with fibre length, though the measurements at 15.2 km showed a shorter coherence time and a higher rms over 500 seconds, perhaps reflecting larger temperature variations than for the other runs. The time scale for the thermal drift to start to dominate does not seem to vary consistently with fibre length, again indicating that environmental conditions dominate here.

Note that H masers have typical values for the Allen standard deviation for a lag of 10 seconds of 1×10^{-14} to 1×10^{-13} , with the Sigma Tau maser used at JBO expected to have an Allen standard deviation of 2×10^{-14} . The values we obtained are consistent with that figure for 2-m fibre, and are up to a factor of 3 or so worse for 30 km.

The long-term stability of a maser is of course much better (10^{-15} at 1000 seconds) than that shown by the fibre link. The results show clearly that some method of compensation for thermal drift in the fibre, by for example a go-and-return phase measurement system as for the radio links currently used in MERLIN, must be used if fibres are to be used as part of a local oscillator coherence system. We conclude that provided this is implemented then fibres can be used to distribute local oscillator signals coherently over distances of 10's of km. However it is unlikely that they can be used for this function when in a 1000 km network subject to arbitrary path switching in an installed and shared high capacity data link system.

4) References

Thompson, A. R., Moran, J. M., and Swenson, G. W., 'Interferometry and Synthesis in Radio Astronomy', Wiley, New York, 1986.

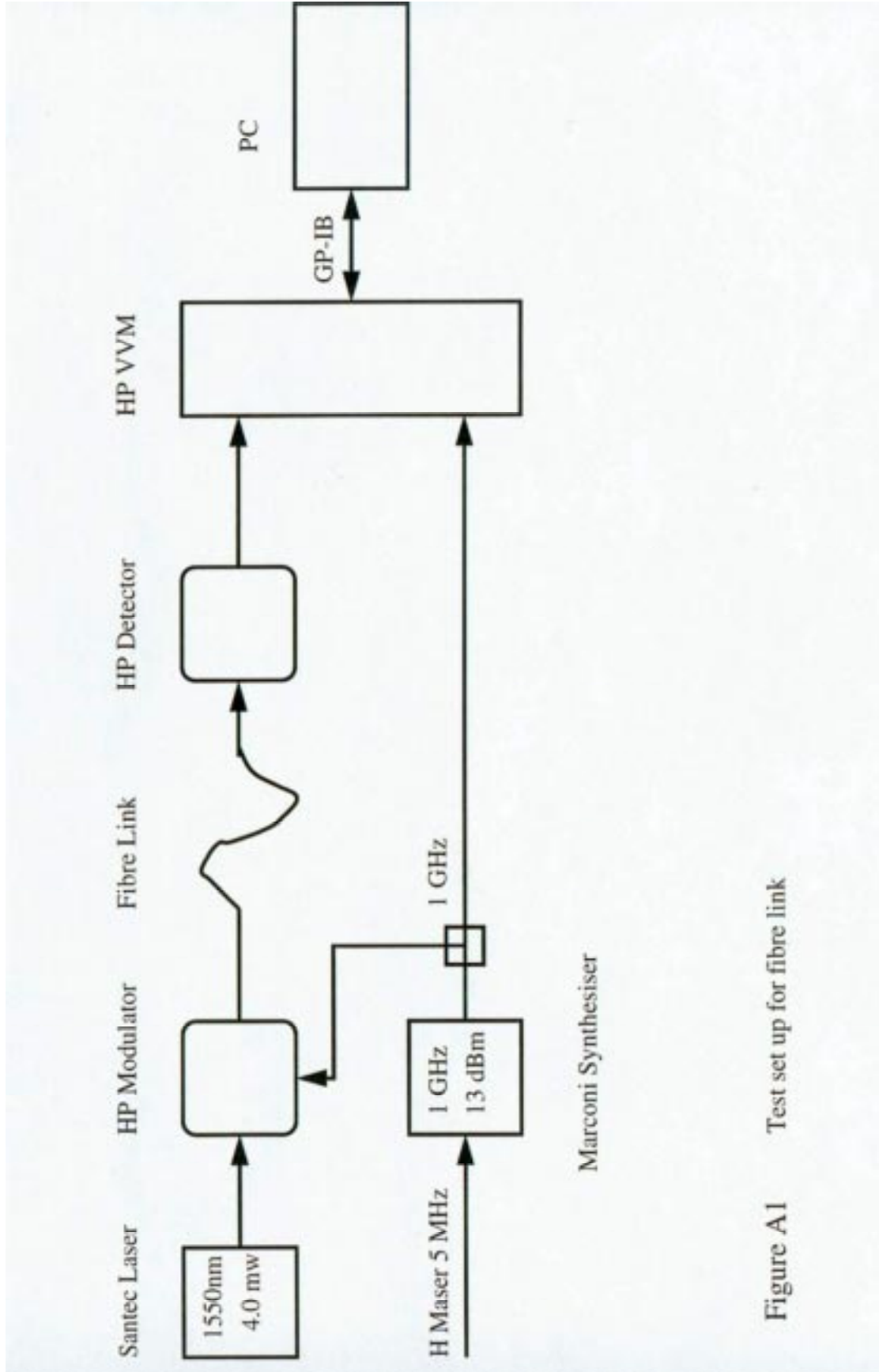


Figure A1 Test set up for fibre link

Figure 2 Plot of phase data for run 200620a.dat

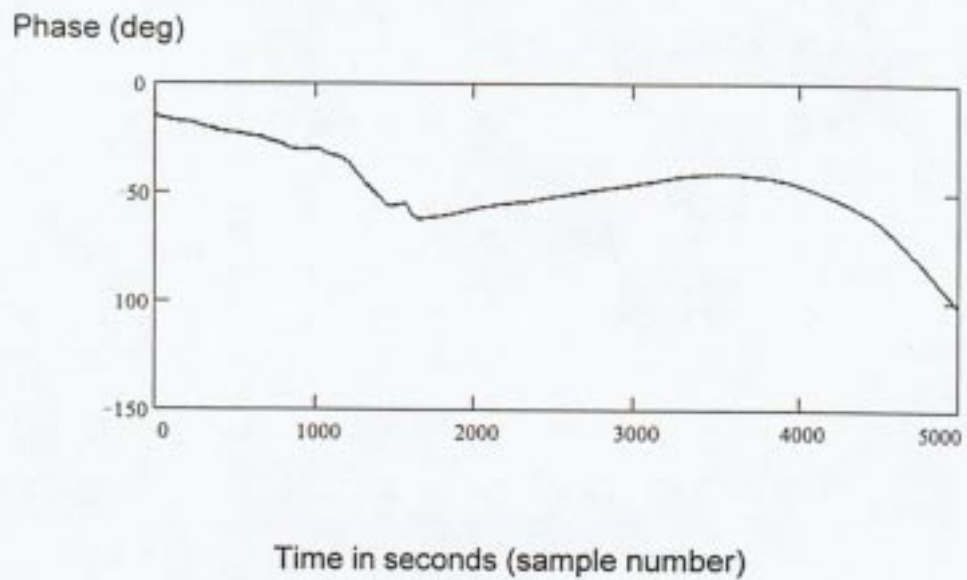


Figure 3 Allen Standard Deviation vs Lag

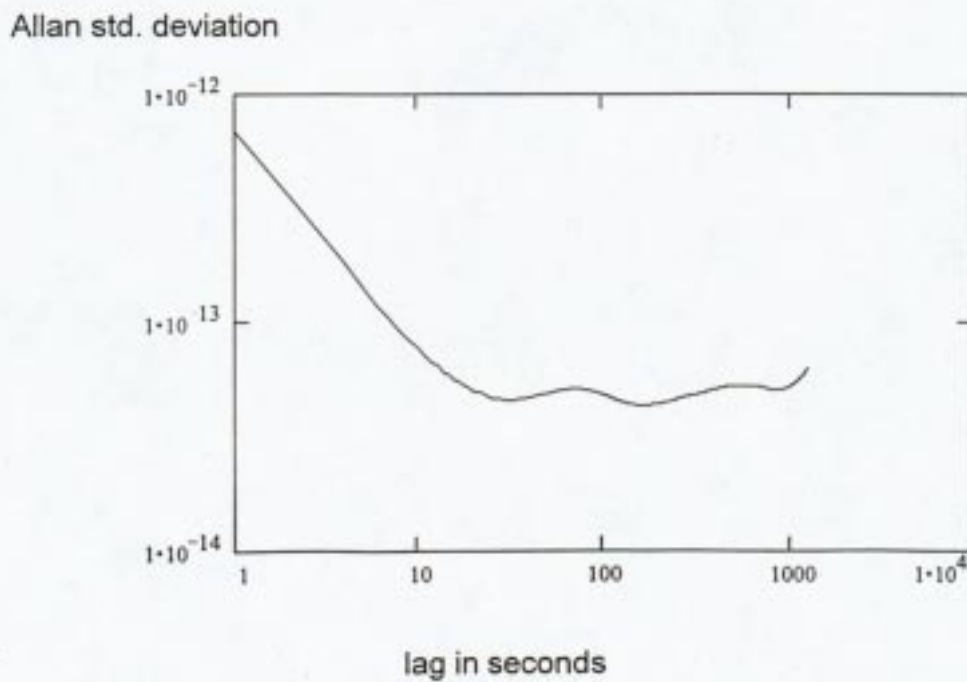
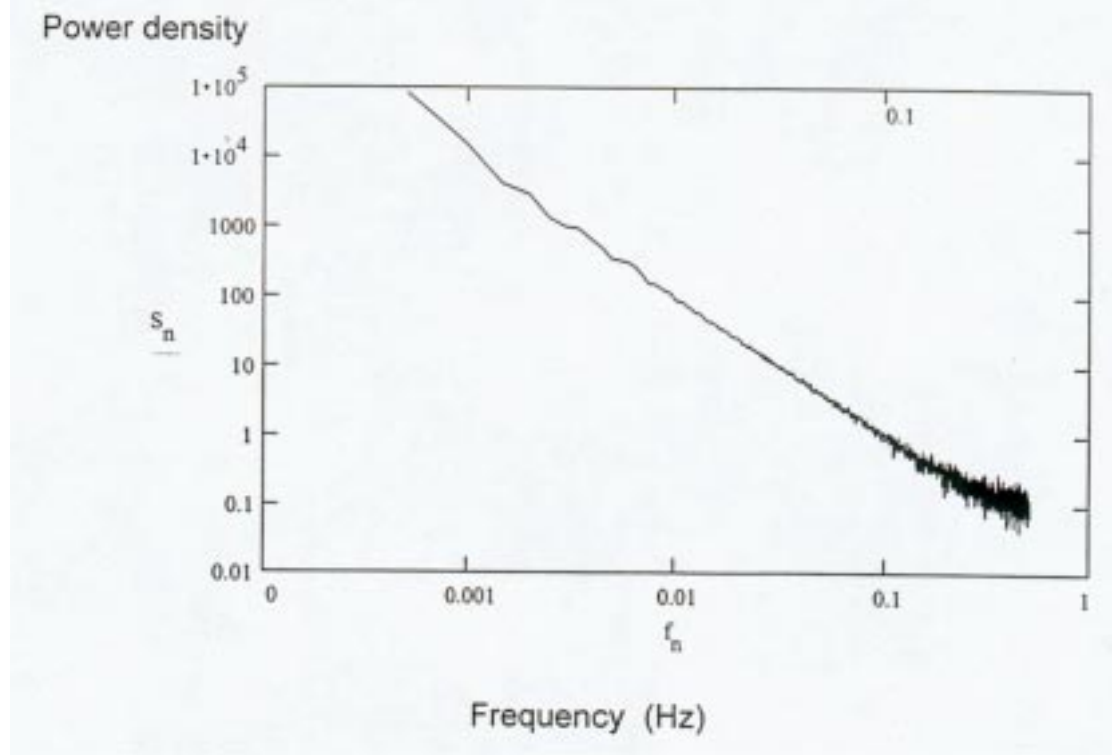


Figure 4 Power Spectrum of Phase fluctuations



APPENDIX B. THE SDH AND SONET STANDARDS

B1. Introduction

SONET and SDH are the standards used to combine a mixture of different types of tele-communications traffic onto a single high bandwidth optical fibre or radio channel. SONET (Synchronous Optical Network) is an ANSI standard originally developed for North America and the Far East. SDH (Synchronous Digital Hierarchy) is an international standard set by the CCITT (now the ITU). It is often regarded as a European standard because most implementations support only European defined data rates. Both standards feature options for use within their primary spheres of influence.

All the information in this appendix is contained in the formal specifications (Ref 1; Ref 2). The other references have been used to collate and explain the specifications. A list of acronyms is given in section B7.

The basic unit of transmission in SONET is 51.84Mbps but in order to carry existing 140Mbps traffic, as well as looking forward to carrying internet protocol (IP) and asynchronous transfer mode (ATM) traffic, SDH has adopted a base rate of three times this at 155.52Mbps. With the correct choice of options, SONET can be seen as a compatible subset of SDH and thus traffic interworking is possible. However, in general the alarm and performance management features are not compatible. The rest of this appendix will concentrate on SDH

B2. SDH

The important features of SDH are contained within its name. It is synchronous and it is hierarchical. A non-synchronous system requires the insertion of justification bits to match the data rates between channels originating in different pieces of equipment. The presence of these justification bits in the data stream makes it impossible to locate a single channel within the stream without completely demultiplexing it. Thus, dropping or inserting a channel requires substantial amounts of hardware. A fully synchronous system avoids this problem, as the location of a channel within the stream is well defined.

Of course, in practice it is impossible to configure a very large switched network to be fully synchronous. Although very accurate atomic clocks are used to generate a primary frequency standards, which are distributed and regenerated around the network some phase and frequency wander are inevitable. SDH uses an ingenious system of pointers, described below, to overcome this problem.

SDH is hierarchical in two senses. The basic transmission frame contains a top-level payload frame which can contain a hierarchy of smaller frames, the lowest level being the actual line traffic. Top-level frames can be combined to form higher levels of the hierarchy.

There is also a hierarchical layer model. The lowest layer is the physical layer which represents the transmission medium. This is usually an optical fibre or possibly a

satellite or radio link. The next layer is the regenerator section, the path between regenerators. The multiplexer section is the section between multiplexers, where signals can be added or dropped. The highest layer is the path which is the end to end connection for a signal. Overhead is added to both section and path layers for control and signalling within the layer.

B3. Frame Structure

The base data transmission frame, known as STM-1 (synchronous transport module) consists of 2430 bytes with a repeat period of 125µs - the same as established PCM - giving a gross transport rate of 155.52 Mb/s. Conventionally the frame is represented as a matrix of 270 rows of nine columns (figure B1) , each byte being equivalent to 64Kb/s - the established standard for a single voice channel.

The first nine columns contain the section overhead (SOH). This has facilities for framing, line operation, administration and maintenance (OA&M), and error monitoring for the regenerator and multiplexer layers. The SOH also contains the pointer to the highest level payload frame. The remaining columns are allocated as required to carry a mix of lower data rate signals. Payload capacity for these signals occupies an integral number of columns and each signal has its own management information called the path overhead (POH).

The highest level division is the administrative unit (AU) which comes in various sizes. The largest, AU-4, occupies the entire payload capacity of an STM-1 and can carry a 140Mb/s signal. 45Mb/s signals are allocated a smaller unit, an AU-3, and three of these are grouped into a group (AUG) which, again, fully occupies an STM-1.

An AU can be further divided to carry slower traffic. These divisions are known as tributary units (TUs) which come in various sizes to match different traffic rates. A TU-12, for example, carries a single 2Mb/s signal and occupies four columns. A TU-2, occupying 12 columns, carries a 6Mbps signal, as used in North America and Japan. TUs can be combined into groups called, inevitably, TUGs. TUGs do not carry any overhead and exist only by virtue of network management tracking their path.

B4. Virtual Containers

At each level units of capacity can float between the payload areas of adjacent frames. This is the method used to cope with variations of frequency and phase. Each subunit can be easily found from its own pointer, which is contained within the overheads (Figure B2). This pointer identifies the start of the floating part of the AU or TU, which is called a virtual container (VC). The AU pointer, contained in the SOH, locates the highest order VC and the TU pointers locate lower order VCs. For example, an AU-3 contains a VC-3 and a pointer; a TU-2 contains a VC-2 and a pointer.

A VC is the fundamental unit which travels unchanged over the network path, being created and dismantled near the termination points. Synchronous traffic is mapped

into a container of the correct size for its data rate using single bit justification to align the clock rate. A VC is formed by adding a POH for management control. Several VCs of the same nominal size are then multiplexed by byte interleaving into the SDH payload. The overheads are removed when the VC is dismantled and the original signal recovered.

Although ATM traffic is supposed to consist of discontinuous 53 byte cells, in practice the gaps are filled by ATM idle cells when the signal is routed onto an SDH interface. The continuous signal so formed can then be handled in the same manner as synchronous traffic

.B5. Higher Data Rates.

Higher levels of the hierarchy are formed by interleaving, at the byte level, the payload from a number, N, of STM-1 signals. A transport overhead N times the size of that of an STM-1 is then added and populated with new management data and pointers. The resultant transmission module is called an STM-N. N is always a multiple of four and has no theoretical upper limit. STM-16 for example runs at 2.48832Gbp/s and can carry 16 x AU-4.

Figure B3 summarises the processes for all the synchronous rates supported by SDH. Other rates and services can be dealt with by concatenation. This process allows multiples of higher or lower order VCs to be managed as if they were a single VC. N VCs are linked by setting their pointers to the same value and each VC is sent on one of the constituent STM-1s. For example, four VC-4s can be concatenated to give a circuit capacity of over 600Mb/s. This is called VC4-4c.

Before transmission, the STM-N signal is scrambled to randomise the bit sequence which improves transmission performance by (minimising the maximum run length). Framing bytes in the overhead are not scrambled. Broadband payloads, in particular ATM cells require a longer scrambling sequence than that originally specified for synchronous signals.

B6. SDH/SONET Convergence

SDH and SONET converge at SONET's 52Mbps base level STS-1. The base level for SDH is STM-1 which is equivalent to SONET's STS-3. By changing the SONET standard from bit interleaving to byte interleaving it became possible for SDH to accommodate both transmission hierarchies. SDH did away with a number of the lower multiplexing levels below 2Mbps. Tables B1 and B2 show how the various data rates are integrated.

Figure 1: SDH Frame

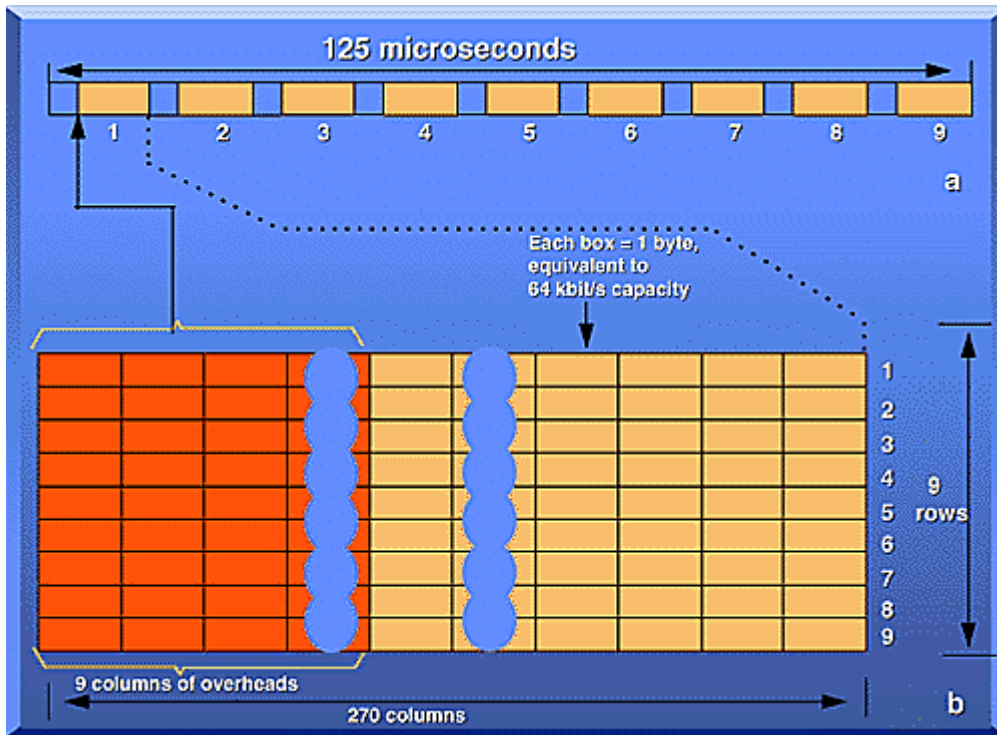


Figure 2: Payload Capacity

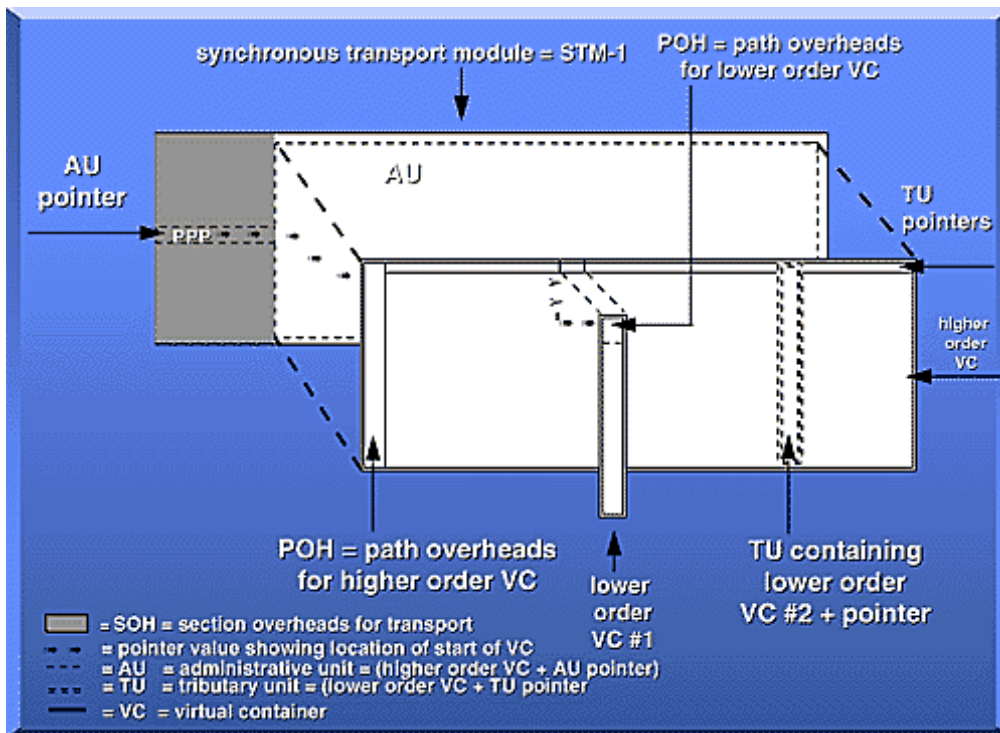


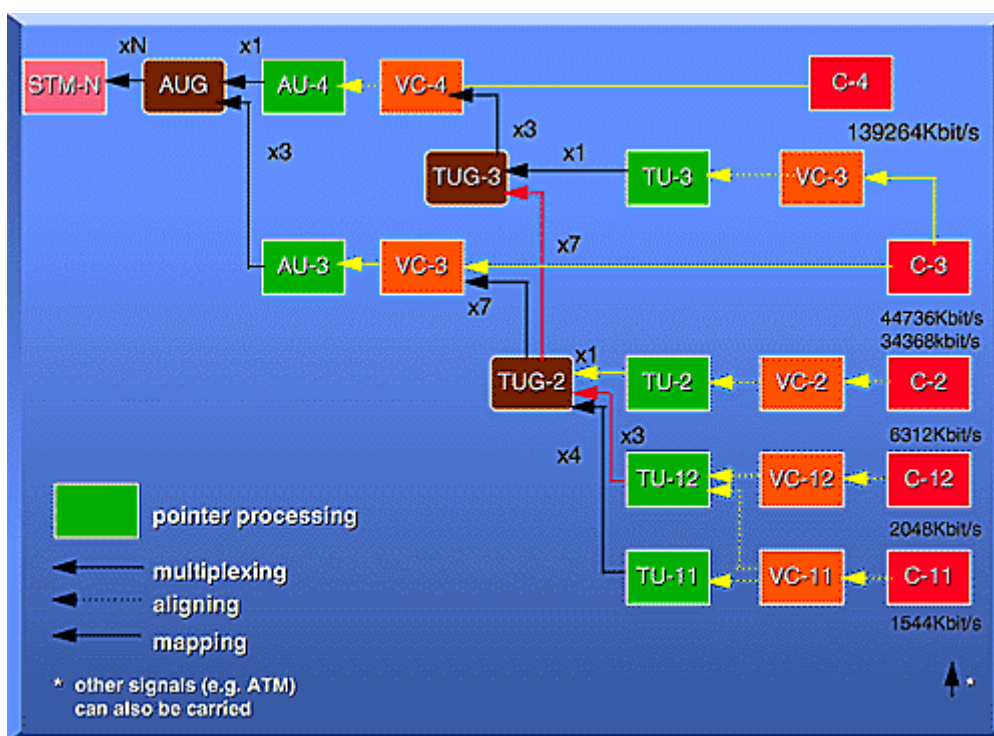
Table B1: Non Synchronous Hierarchies

ANSI RATE			ITU-U RATE		
Signal	Bit Rate	Channels	Signal	Bit Rate	Channels
DS0	64 Kbps	1xDS0	64Kbps	64 Kbps	1X64K
DS1	1.544 Mbps	24xDS0	E1	2.048 Mbps	1xE1
DS2	6.312 Mbps	96xDS0	E2	8.450 Mbps	1x64K
DS3	44.736 Mbps	28xDS1	E3	34.368 Mbps	16xE1
			E4	139.264 Mbps	64xE1

Table B2: SDH/SONET Hierarchies

SDH Signal	Bit Rate	SONET Signal	SDH Capacity	SONET Capacity
STM-0	51.840M	STS-1 OC-1	21xE1	28xDS1 1xDS3
STM-1	155.520M	STS-3 OC-3	63xE1 1xE4	84xDS1 3xDS3
STM-4	622.080M	STS-12 OC-12	252xE1 4xE4	336xDS1 12xDS3
STM-16	2488.320M	STS-48 OC-48	1008xE1 16xE4	1344xDS1 48xDS3
STM-64	9953.280M	STS-192 OC-192	4032xE1 64xE4	5376xDS1 192xDS3

Figure 3: ITU-TS Multiplexing Structure



B7. Acronym Guide

ADM	Add-drop multiplexer
ANSI	American National Standards Institute
ATM	Asynchronous transfer mode - a form of fast short packet switching and multiplexing
AU	administrative unit - a managed entity within the SDH structure
BISDN	Broadband integrated services digital network
CCITT	Comité Consultif International Telegraphique et Telephonique - in English Consultative Committee on International Telegraphy and Telephony - predecessor of ITU-TS11
DCC	Data communications channel - the main management channel inside SDH
DCS	Digital cross-connect system - an electronic multiport switch for digital traffic
DXC	Digital cross-connect - see DCS
ETSI	European Telecommunications Standards Institute
FDDI	Fibre distributed data interface - a short range 100 Mbps interface used between large computing nodes
IDLC	Integrated digital loop carrier - a North American system for connecting an exchange/central office to subscribers over a large area via fibre
IP	Internet protocol - a component of protocol for many computer links including the Internet
ITU-TS	International Telecommunications Union-Transmission Standards
LAN	Local-area network - a linked group of computers
MAN	Metropolitan-area network - an area network for public broadband traffic
NNI	Network node interface - a defined interface between nodes in the public network
PDH	Plesiochronous digital hierarchy - the widely deployed transmission system which predates SDH
POH	Path overhead - a group of management communications facilities in SDH
SDH	Synchronous digital hierarchy
SOH	Section overhead - a group of management communications facilities in SDH
SONET	Synchronous optical network - the North American variant of SDH
STM	Synchronous transport module - the basic unit of transmission in SDH
TU	Tributary unit - the basic unit of payload together with its management overheads and synchronisation data
TUG	Tributary unit group - a managed group of TU
UNI	User-network interface - a defined interface between the user and the public network
VC	Virtual container - the basic unit of payload together with its management overheads

B8. References

- [1] International Telecommunications Union Standards.
- [a] ITU-T G.707: Network Node Interface for the Synchronous Digital Hierarchy (SDH)
 - [b] ITU-T G.781: Structure of Recommendations on Equipment for the Synchronous Digital Hierarchy (SDH)
 - [c] ITU-T G.782: Types and Characteristics of Synchronous Digital Hierarchy (SDH) Equipment
 - [d] ITU-T G.783: Characteristics of Synchronous Digital Hierarchy (SDH) Equipment Functional Blocks
 - [e] ITU-T G.803: Architecture of Transport Networks Based on the Synchronous Digital Hierarchy (SDH)
- [2] American National Standards Institute Standards.
- [a] ANSI T1.105: SONET - Basic Description including Multiplex Structure, Rates and Formats
 - [b] ANSI T1.105.01: SONET - Automatic Protection Switching
 - [c] ANSI T1.105.02: SONET - Payload Mappings
 - [d] ANSI T1.105.03: SONET - Jitter at Network Interfaces
 - [e] ANSI T1.105.03a: SONET - Jitter at Network Interfaces - DS1 Supplement
 - [f] ANSI T1.105.03b: SONET - Jitter at Network Interfaces - DS3 Wander Supplement
 - [g] ANSI T1.105.04: SONET - Data Communication Channel Protocol and Architectures
 - [h] ANSI T1.105.05: SONET - Tandem Connection Maintenance
 - [i] ANSI T1.105.06: SONET - Physical Layer Specifications
 - [j] ANSI T1.105.07: SONET - Sub-STS-1 Interface Rates and Formats Specification
 - [k] ANSI T1.105.09: SONET - Network Element Timing and Synchronization
 - [l] ANSI T1.119: SONET - Operations, Administration, Maintenance, and Provisioning (OAM&P) - Communications
 - [m] ANSI T1.119.01: SONET: OAM&P Communications Protection Switching Fragment
- [3] M.Jeffrey; Synchronous Transfer Mode: The Ultimate Broadband Solution; IEE Electronics and Communication Journal, June 1994
- [4] QUB; SDH/SONET; The Queen's University of Belfast Parallel Computer Centre (<http://www.pcc.qub.ac.uk/tec/courses/>)
- [5] Rad Data Communications; SDH Tutorial; (<http://www.rad.com/networks/netterms.htm>)
- [6] Tektronix: Synchronous Optical Network (SONET) Tutorial; International Engineering Consortium Web Proforum Tutorial (<http://www.iec.org>)
- [7] SDH Pocket Guide Volume 1; Wandel and Goltermann.

APPENDIX C: TRANSFER OF VLBI SIGNALS TO SDH

C1 Introduction.

It is unlikely that a European wide fibre link system would give full access to dark fibre at the observatory sites. Instead access to a standard commercial system is more likely, and in particular to an SDH system. This is expected to provide the data transport infrastructure for the next 2 or 3 decades and is likely to form the basis for any terabit system envisaged for interconnection of major European large-scale scientific facilities.

A description of technical aspects of SDH was given in Appendix B. This appendix addresses the problem of how VLBI data can be presented to an SDH link, without going into detailed design.

C2 VLBI Data Formats.

The recording systems used for VLBI consist of the VLBA and MKIV standards which basically give 32 data streams at 32 Mbps maximum, giving 1 Gbps maximum data rate. This can be increased by the addition of further hardware to 2 Gbps, but this is not envisaged at the moment. Lower data rates are also used depending on the observing mode. Analogue signals from the radio receivers are split in the VLBA data acquisition rack (DAQ) into multiple basebands. For the VLBA system this is limited to 16 bands of up to 16 MHz bandwidth each. The MkIV system can have 28 such bands. These signals are then sampled at the Nyquist rate at 1 or 2 bits per sample. The maximum data rate of 1 Gbps therefore means a bandwidth of 512 MHz for 1 bit (32 bands of 16 MHz), or 256 MHz (16 bands). Current hardware therefore limits existing systems in EVN to 256 MHz and 2 bit sampling. The samplers are external for VLBA system but internal to the data formatter for MKIV. The formatter adds header information and timing data, and constructs signals for use in recording onto magnetic data. The output of the formatter consists of 64 data streams at 18 Mbps each on balanced lines with standard emitter coupled logic signals, and non-return-to-zero (NRZ) encoded. These signals are normally sent to the tape recorder which lays 64 tracks (on two headstacks) longitudinally recorded onto magnetic video tape. A full description of data formats is given in the MkIV memos from MIT Haystack observatory, USA., particularly memo no. 205.6 (Whitney 1995).

C3 Transfer of VLBI Data Onto a Link.

a) A Simple Approach?

The standard data rates for SDH systems are at multiples of the standard STM1 rate of 155.52 Mbps. Two 622 Mbps STM4 channels would cope with existing maximum data rates, and 4 such channels would allow expansion for higher data rates in future.

The simplest transfer method with the minimum build of new hardware is outlined in figure C1, where the output of the formatter is taken directly. 8 x 18 Mbps channels

need to be framed into a standard STM1 signal. 4 such data streams can be assembled into a 622 Mbps STM4 signal and then subsequently incorporating 2 such channels onto the SDH link by using standard equipment. Note that the next higher bandwidth SDH standard is SDH16 at 2.5 Gbps, there is therefore spare capacity (probably shared with other users) on such a link.

The hardware to put the 18 Mbps signals into STM1 format is not available commercially due to the non-standard data rate and therefore requires some design and construction effort. Another problem is that the maximum raw data rate in a 155.52 Mbps STM1 signal is actually lower due to the overhead in the SDH system, and in fact is 140 Mbps, compared with $8 \times 18 = 144$ Mbps. There will therefore be missing data with this simple approach unless a way of removing some of the redundant timing information in the formatted VLBI signals (the time is duplicated in each channel) can be used. This is likely to pose a difficult design problem, and data loss is likely, resulting in poorer signal to noise at best and loss of timing (hence delay) information at worse.

This simplistic method is therefore not recommended.

b) Use of the New VLBI Standard:

A new approach to the problem of interconnectability of VLBI equipment has been undertaken recently by an international team led by Haystack observatory. A VLBI standard interface (VSI) has been defined, in both hardware (VSI-H) and software (VSI-S). The document defining VSI-H has been completed (VSI-H 2000) and will shortly be accessible on the web. This system supports 32 data streams at clock rates of up to 32 MHz and includes control and timing signals. The data transfer system includes a data input module (DIM) which converts the incoming multiple parallel data streams into a form suitable for the transmission medium including time-tagging, and a data output module (DOM) which accepts data from the transmission medium and presents the data streams to the correlator. Cable and connector specifications are included along with control interfaces in the definition, but data formats for the transmission medium are not.

Figure C2 shows a scheme for taking data for transferring data to and from an SDH link using the VSI-H components. Design work is again needed here, particularly for the data framing and de-framing required to produce SDH signals. However devices exist for the standard (32 MHz) signals envisaged here (e.g. the AMCC S2065 serial backplane device) and so should not be too difficult. The only problem for existing VLBI equipment is that the data streams at 32 MHz have to be generated from the sampled data. This is straightforward for the VLBA style of formatter since the samplers are external, however either new samplers or a modification to the existing formatter enabling access to the sampled signals are required.

This approach is recommended as it will maintain compatibility with future VLBI systems.

C4 Further Work

If implementation of an EVN wide fibre network is carried out then a detailed design of the digital electronics required in the DIM and DOM units for data conversion is required. This may take 0.5 – 1 man year of effort for an engineer. Around 12 DIM units for the VLBI stations will be required with a corresponding 12 DOM units at the correlator. These are likely to be produced commercially and cost several thousand Euros each. A working group which maintains contact with fibre providers and the organisation responsible for implementing the tera-bit network (possibly DANTE) will be required.

C5 References

VSI-H 2000, Proposed VLBI Standard Hardware Interface Specification, MIT Haystack Observatory, May 2000, (contact awhitney@haystack.mit.edu).

Whitney 1995, Mark IV Memo no. 205.6, Mark IV Tape Format, Recording Modes and Compatibility, A.R. Whitney, June 1995.

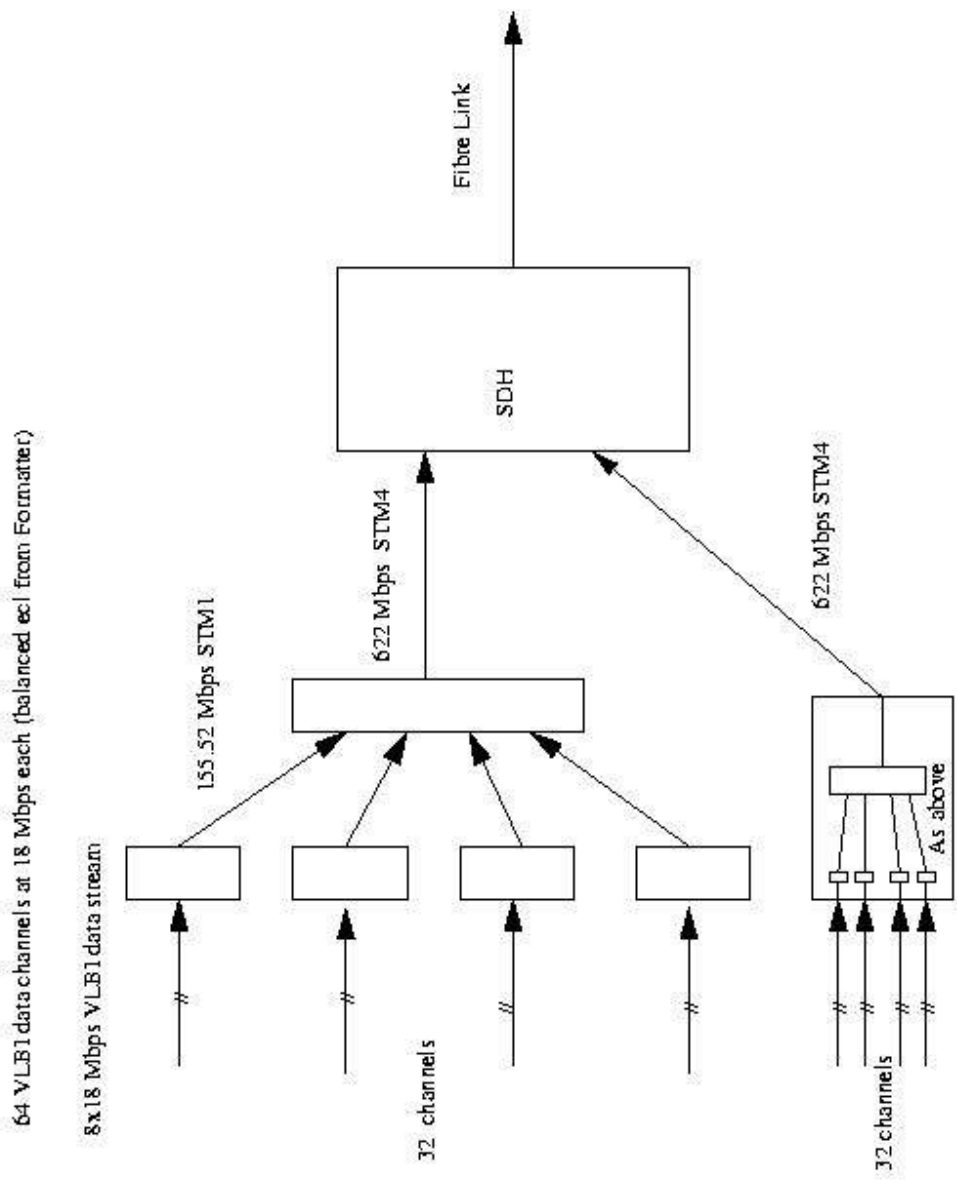


Figure C1 Transfer of VLBI data onto SDH Link

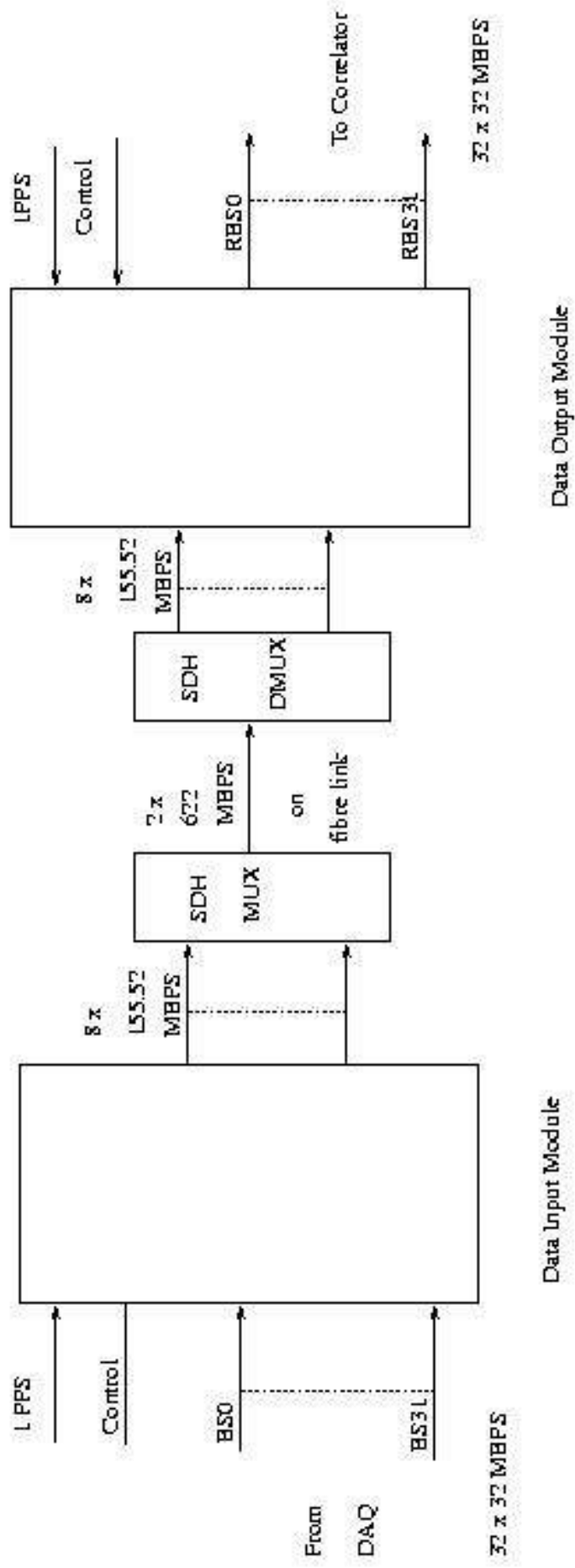


Figure C2 Transferring VLBI signals to fibre link using VSL-H system

